

AUGER ELECTRON DOSIMETRY



AUGER ELECTRON DOSIMETRY

INTRODUCTION

James G. Kereiakes and Dandamudi V. Rao

BIOLOGICAL EFFECTS OF THE AUGER EMITTER IODINE-125

Kandula S. R. Sastry

RADIATION SPECTRA FOR AUGER-ELECTRON EMITTING RADIONUCLIDES

Roger W. Howell

REPORT OF
TASK GROUP NO. 6
AAPM NUCLEAR MEDICINE COMMITTEE

Members

James G. Kereiakes
Dandamudi V. Rao
Kandula S. R. Sastry
Roger W. Howell

*Reprinted from MEDICAL PHYSICS, Vol. 19, Issue 6, 1992

January 1993

Published for the
American Association of Physicists in Medicine
by the American Institute of Physics

DISCLAIMER: This publication is based on sources and information believed to be reliable, but the AAPM and the editors disclaim any warranty or liability based on or relating to the contents of this publication.

The AAPM does not endorse any products, manufacturers, or suppliers. Nothing in this publication should be interpreted as implying such endorsement.

Further copies of this report (\$10 prepaid) may be obtained from:

American Institute of Physics
c/o AIDC
64 Depot Road
Colchester, Vermont 05446

(1-800-488-2665)

International Standard Book Number: 1-56396-186-5
International Standard Serial Number: 0271-7344

©1993 by the American Association of Physicists in Medicine

All rights reserved. No part of this publication may be reproduced, stored in a retrieval system, or transmitted in any form or by any means (electronic, mechanical, photocopying, recording, or otherwise) without the prior written permission of the publisher.

Published by the American Institute of Physics, Inc.
335 East 45th Street, New York, NY 10017-3483

Printed in the United States of America

Auger electron dosimetry: Report of AAPM Nuclear Medicine Committee Task Group No. 6^{a)}

James G. Kereiakes
University of Cincinnati, Cincinnati, Ohio 45267

Dandamudi V. Rao
University of Medicine and Dentistry of New Jersey, New Jersey Medical School, Newark,
New Jersey 07103

(Received 16 March 1992; accepted for publication 7 May 1992)

Several radionuclides used in nuclear medicine decay by electron capture and/or internal conversion (^{201}Tl , ^{123}I , ^{111}In , ^{67}Ga , $^{99\text{m}}\text{Tc}$, etc.). As a consequence of the inner atomic shell vacancy created by these decay modes, several Auger electrons are emitted per decay. Most of these electrons have very low energies (~20-500 eV) with ranges of the order of subcellular dimensions in tissue. Accordingly, highly localized energy deposition occurs around the decay sites. Many experiments *in vitro* and *in vivo* have clearly demonstrated that the biological effects of such electrons can be significantly higher than expectations based on the average absorbed dose (MIRD method) to the organ. Consequently, the dosimetry of incorporated radionuclides that emit Auger electrons has drawn considerable attention from the medical community. The conventional procedures of calculating the average absorbed dose to the organ may not be adequate to assess the risk associated with procedures involving incorporated radionuclides which are Auger emitters. The increasing use of such radionuclides as diagnostic agents, in conjunction with their use in the treatment of cancer (e.g., radiolabeled monoclonal antibodies), emphasizes the need for dosimetry techniques that may predict the biological response more realistically. Recognizing this need, the American Association of Physicists in Medicine (AAPM), established in 1989 the Auger Electron Dosimetry Task Group No. 6 under the auspices of the Nuclear Medicine Committee, Science Council, to informally discuss methods to calculate the "relevant" absorbed dose from incorporated Auger-electron emitting radionuclides. The responsibilities of the task group were: (1) review the current status of research in this field, (2) discuss whether the dose to cell populations within the organ is more relevant than the average organ dose, (3) suggest additional biological data that may be necessary for Auger electron dosimetry, (4) compile and publish complete Auger electron spectra for radionuclides used in medicine, and if necessary calculate spectra for radionuclides for which there are no published data, (5) recommend procedures to calculate the relevant dose from diagnostic

and therapeutic administration of Auger emitters, and (6) disseminate the Committee findings to the scientific community through Committee reports and publications.

The most extensively investigated radionuclide to study Auger-electron effects has been ^{125}I , which emits numerous low-energy electrons. The committee felt that a review of the extensive literature available on the biological effects of ^{125}I *in vitro* and *in vivo* would introduce the problem of Auger-electron dosimetry to the reader and underscore the need for methods to properly predict the biological effect. Accordingly, the first of the two reports presented in this issue of *Medical Physics*, primarily prepared by Kandula S. R. Sastry and reviewed and revised by the committee, is entitled "Biological effects of the Auger emitter ^{125}I -A review." This review is not intended to be exhaustive, but rather provide an overview of the research in this field.

The second report, primarily prepared by Roger W. Howell and reviewed by the committee, is entitled "Radiation spectra for Auger-electron emitting radionuclides." The data contained therein are valuable for medical physicists who are interested in the microdosimetry of Auger-electron emitters. Although spectra for some of these radionuclides may already be available in the literature, the data presented in this report provide a set of spectra calculated in a self-consistent manner. These spectra give the necessary information for medical physicists to calculate the absorbed dose at the subcellular level for these radionuclides.

The task group is presently preparing a third report which reviews the different approaches to Auger-electron dosimetry and makes recommendations regarding practical methods to predict the biological response that may be useful in clinical settings. This report will appear in a later issue of *Medical Physics*.

^{a)}James G. Kereiakes, Co-Chairman, Dandamudi V. Rao, Co-Chairman, Roger W. Howell, John L. Humm, Ravinder Nath, Kandula S. R. Sastry, Sven-Erik Strand, and Stephen R. Thomas

Biological effects of the Auger emitter iodine-125 A review. Report No. 1 of AAPM Nuclear Medicine Task Group No. 6^{a)}

Kandula S. R. Sastry

Department of Physics and Astronomy, University of Massachusetts, Amherst, Massachusetts 01003

(Received 16 March 1992; accepted for publication 23 July 1992)

The biological implications of Auger electron cascades following inner shell ionization of atoms have been of interest for over 25 years. By virtue of their decay via orbital electron capture and/or internal conversion, several biomedical radionuclides emit numerous low-energy electrons spontaneously. The biological effects of such radionuclides incorporated into tissues cannot be predicted *a priori* because of the highly localized patterns of energy deposition by the electrons. Results of extensive research using Iodine-125 as a model Auger electron emitter are now available. This article presents an up-to-date review of the physical and radiobiological data on this Auger emitter. Valuable concepts concerning the action of internal Auger emitters are identified phenomenologically, and questions that need to be answered are indicated. The present understanding provides a scientific basis toward estimation of risk associated with Auger emitters used in diagnosis, and suggests potential applications to therapy.

I. INTRODUCTION

A. Auger processes

When an atom is ionized in its inner atomic shell, the excited residual atom quickly returns to a stable configuration via radiative (R) and nonradiative (NR) processes. The former involves emission of characteristic atomic x-ray photons, while the NR cascade transitions result in the ejection of atomic electrons via Auger, Coster-Kronig (CK) and super CK processes, in general.¹⁻⁴ These NR processes are illustrated in Fig. 1, and we denote the ejected electrons as Auger electrons, first observed by Pierre Auger⁵ in cloud chamber experiments when rare gases were exposed to x-rays. In addition to the external photoelectric effect, physical decay of radionuclides by orbital electron capture (EC) and by internal conversion (IC) also entail inner atomic shell ionization. Such radionuclides are often called Auger emitters; and I-125, which decays by EC followed quickly by IC, has been a popular example.

B. Biophysical implications of Auger electrons

Auger cascade electrons display a very complex energy spectrum, dominated by a large number of very low-energy electrons (~20-500 eV) with ranges (~1-10 nm) of macromolecular dimensions in biological matter.³⁻⁶ Although the linear energy transfer (LET) of these electrons is about 10-25 keV/ μm , their simultaneous action may simulate high-LET-type biological damage, comparable with the effects of densely ionizing a particles of high LET. The localized effects of Auger cascades cannot be predicted *a priori*. Nevertheless, there is now overwhelming evidence that Auger cascades can cause severe biological damage both *in vitro* and *in vivo*, even though the low-energy electrons carry only a small fraction of the total amount of energy associated with the primary physical process.⁷⁻⁹ In view of the widespread use of Auger emitters in diagnostic nuclear medicine, and the fact that conventional dosimetry

of incorporated radionuclides^{10,11} ignores the potential importance of low-energy electrons, it is imperative that we understand the effects of internal Auger emitters at the basic level. The insights thus obtained should be of much value to radiation risk assessment, development of radiopharmaceuticals suitable for diagnosis and therapy, and to an advancement of photon activation therapy (PAT) by utilizing external photoelectric effect to induce Auger cascades in selectively targeted atoms (e.g., iodine) in the DNA of cells.

II. IODINE-125: A PRIME EXAMPLE

Each Auger emitter is unique by virtue of its nuclear decay scheme. Since I-125 has been very extensively investigated from a number of interdisciplinary perspectives, we will use this radionuclide as our model. Rather than being compendious, we will identify the various aspects of particular interest, the understanding gained so far, and questions that need to be clarified.

A. Decay of I-125

The two-step nuclear decay, I-125 (EC) \rightarrow Te-125m (IT) \rightarrow Te-125, is well investigated.¹² The first step involves emission of K x-rays and Auger electrons. The isomeric state has a half-life of about 1.5 ns, and the isomeric transition (IT) is dominated by IC (93%). The EC and IC decay probabilities involving the various atomic subshells are quite well known. The "size of the Auger effect" associated with EC, and with IC is nearly the same. Thus the two-step I-125 decay may be viewed as two approximately equivalent Auger decays that are inseparable. The only difference is that internal conversion electrons and 35.5-keV photons are also emitted in the second step, the respective probabilities being 93% and 7%. The energies and yields of these radiations are well established (see Table I), and disagreements, if any, are of a minor nature. This is

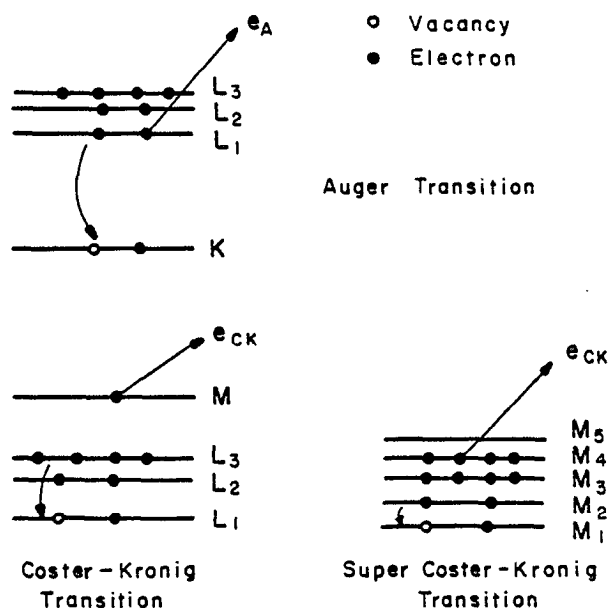


FIG. 1. Types of nonradiative transitions. In R transitions, a photon is emitted and the vacancy moves to a higher shell (not shown). For Te ($Z = 52$), this mechanism is dominant only for an initial K hole. NR transitions (A, CK and super CK) govern the relaxation of vacancies in the L shell and above. For each vacancy filled by these processes, two vacancies are created. In an A transition, an electron is ejected from a higher *major* shell. In a CK transition, a vacancy in a subshell is filled by an electron in a higher subshell in the *same* major shell, with the ejection of an electron from a *higher major shell*. A super CK transition differs in that the ejected electron is from the *same major shell*. When energetically possible, CK and super CK transitions dominate over the A type, and further amplify the vacancy multiplication. There are no CK transitions associated with K-shell vacancies. The NR transitions are denoted by a three-letter code representing the vacancy state, state of the electron filling the vacancy followed by the state from which an electron is ejected. The Auger transition shown in the figure is of the KL_iL_i type, and KLL stands for all possible transitions involving a K-hole and L-shell electrons. The CK transition is of type L_iL_jM , an electron being ejected from one of the five M subshells. The super CK transition shown is denoted by $M_iM_jM_k$ in this notation.^{1,3,4}

also true regarding the K x-ray emissions. L x-ray emissions are small; M x-ray yields are smaller even for heavy elements.

B. Auger electron spectrum

The *complete* Auger and CK electron spectrum has not been measured for I-125, or for any other Auger emitter. Reliable experimental data are available for I-125 for the K and L Auger spectra. The rest of the spectrum has to be calculated using theoretical transition rates and energies,¹³⁻¹⁶ approximations and assumptions¹⁷ and phenomenology revealed by experimental and theoretical atomic research in this region of the periodic table. These aspects have been thoroughly discussed in the review article by Sastry and Rao.³

Except for low Z elements, the NR processes are extremely complex as indicated in the legend to Fig. 1. The progression of the Auger cascade to near valence shells results in the emission of a large number of low-energy electrons because of vacancy multiplication and decreasing

TABLE I. Average photon and IC electron spectrum in I-125 Decay.¹⁸ The photon mean free paths for energy absorption in soft tissue range approximately between 5 to 10 cm; See Ref. 22. Electron ranges are based on Cole's work; See Refs. 3 and 23.

Radiation	Yield/decay	Energy (keV)	Range (μm)
Gamma	0.065	35.5	
IC-K	0.80	3.65	0.50
IC-L	0.11	30.6	18.6
IC-MN	0.028	34.7	23.1
$K_{\alpha 1}$	0.751	27.5	
$K_{\alpha 2}$	0.394	27.2	
$K_{\beta 1}$	0.138	31.0	
$K_{\beta 2}$	0.028	31.7	
$K_{\beta 3}$	0.069	30.9	
$K_{\beta 4}$	0.012	31.7	
$K_{\beta 5}$	0.005	31.2	

TABLE II. Auger (A) and CK spectrum: Near valence shell transitions.¹⁸

Transition	Without O-shell feeding		With O-shell feeding	
	energy in keV	(yield/decay)	energy in keV	(yield/decay)
CK LLX	0.218	(0.268)	0.219	(0.264)
CK MMX	0.127	(1.41)	0.127	(1.44)
A MXY	0.461	(3.27)	0.461	(3.28)
CK NNX	0.029	(3.51)	0.030	(3.51)
A NXY	0.029	(4.66)	0.032	(10.9)

TABLE III. Phenomenological Auger and CK electron spectrum.³

Origin of electron group	Yield per decay	Average energy (keV)	Range (μm) in tissue Refs. 3,23
K_A	0.20	24.3	14.0
L_A	1.58	3.27	0.42
$M_{1,2,3A}$	0.24	0.670	0.037
$M_{4,5A}; L_1, M_{1CK}$	3.17	0.475	0.023
$L_1, M_{1,2CK}$	0.13	0.258	0.012
$L_{1,2}, M_{3CK}$	0.29	0.210	0.010
$L_{1,2}, M_{1,2CK}; N_{1A}$	0.35	0.154	0.0075
$L_2, M_{2,3}; N_{1CK}$	0.82	0.110	0.0055
$M_{1,3CK}; N_{4,5A}$	4.66	0.065	0.004
N_{1CK}	0.31	0.048	0.003
$N_{4,5A}; N_{2CK}$	6.14	0.027	0.0015
N_{3CK}	1.36	0.016	<0.001

TABLE IV. Pomplun's spectrum.³⁰

Transition	Yield/Decay	Ave. energy (keV)
A-KLL	0.131	22.47
A-KLX	0.058	26.42
A-KXY	0.0056	30.20
CK-LLX	0.265	0.280
A-LLM	1.24	3.006
A-LMX	0.348	3.655
A-LXY	0.022	4.289
CK-MMX	1.43	0.090
A-MXY	3.30	0.375
A-NXY	3.45	0.032

transition energies. Data in Tables II-IV represent the average electron spectra obtained through different approaches. The complex spectra are summarized by grouping the electrons by the vacancy state initiating the transition and by energy. The differences between the spectra stem from the simplifying assumptions made in order to render the complex problem reasonably tractable.

(a) All the investigators assumed that, in the condensed phase, the excited Te-125m atom after the EC decay is fully recovered well within the nanosecond time scale of its life-time, and that the Auger cascades follow the IC decay in the same manner as after the first step. The electron spectra for the total decay are treated as additive. This assumption may have some effect on the details of the early chemical events involving interactions of the highly reactive free radicals with biomolecules. Our understanding of such events is too rudimentary to warrant further concern at this time.

(b) Theoretical atomic transition rates are calculated^{15,16} in the independent particle model with established neutral atom electron binding energies,^{19,20} although the need to consider multiple vacancy configurations is well recognized. As noted in Ref. 3, McGuire's calculations in the independent particle model constitute the essential first step toward an advancement of our understanding.

(c) Concomitant with the ejection of several electrons, the residual atom is highly positively charged, and a significant amount of potential energy is associated with the ion. Very little is known about the pathways of subsequent relaxation. A *truly isolated* ion may not even recover the normal electronic configuration. In reality, the Auger emitter is often attached to a molecular carrier. Neighboring electrons partly neutralize the ionic charge. Proximity of a number of positive charges may then result in a Coulombic fragmentation of the molecule. Such effects, originally observed by Carlson and White²¹ with small inorganic molecules ($\text{CH}_3^{125}\text{I}$, $\text{C}_2\text{H}_5^{125}\text{I}$) in the rarefied phase, fascinated many to suggest "Coulombic explosion" as a mechanism for biological damage by DNA-incorporated I-125. Studies by Stöcklin and co-workers^{24,25} have shown that this destructive mechanism does occur even in the condensed phase relevant to biology but limited to the small molecule to which I-125 is directly attached (e.g., ¹²⁵Iodouracil). However, their work suggests that the high-LET-type cytotoxic effects of DNA-incorporated I-125 may be primarily due to the simultaneous localized action of the numerous low-energy electrons. Considering that the DNA is highly hydrated, interaction of the Te^{n+} ion with H_2O molecules in its immediate environment should provide a major pathway for charge neutralization. Intermolecular Auger processes are expected to de-excite the ion with the emission of low-energy electrons, and the production of free radicals as the excited water molecule dissociates: $(\text{H}_2\text{O})^* \rightarrow \text{H} \cdot + \text{OH} \cdot$ (Refs. 3 and 24). There is independent evidence for electron and photon stimulated desorption in small molecules via intermolecular Auger processes.^{26,27}

The above remarks convey the essential background concerning the intriguing aspects of the action of I-125,

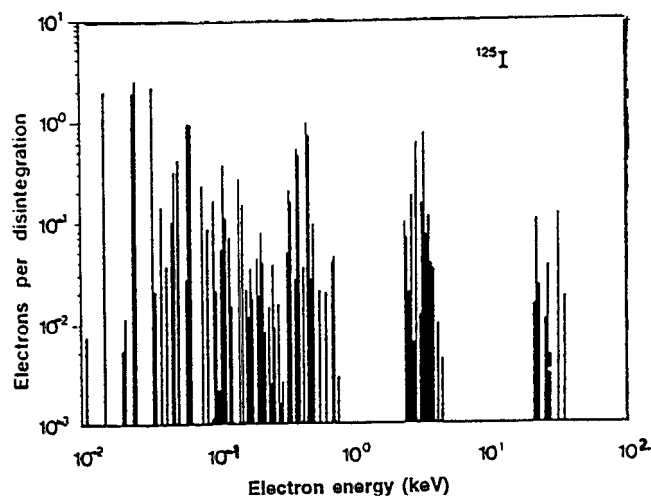


FIG. 2. Electron spectrum in the decay of I-125 calculated by Charlton and Booz.²⁸

and point to the importance of the dosimetry of low-energy electrons at the nanometric level. It is in this context that distinctions between the spectra in Tables II-IV may be relevant.

(i) Charlton and Booz,²⁸ and Howell¹⁸ used Monte Carlo methods^{28,29} and the theoretical transition rates and available binding energies to calculate the Auger and CK spectra. The $Z / (Z + 1)$ rule¹⁷ is used to obtain the transition energies (see Ref. 3 for more details). It is assumed that O-shell vacancies are sufficiently neutralized by the environment.^{3,18,28} Their results are in agreement, with about 21 electrons being ejected, on the average (see Fig. 2). Howell's results¹⁸ in Table II show that the energy spectrum is the same whether the O shell is fed or not fed with electrons except that the yield of NXY Auger electrons is 4.7/decay without O-shell feeding and 10.5/decay with the feeding.

(ii) The approach of Pomplun *et al.*³⁰ uses Dirac-Fock codes of Desclaux³¹ and takes account of multivacancy configurations. They treat the I-125 decay in isolation. The electron spectrum is calculated for the first step using the transition rates in the independent particle model, and the average charge state and the potential energy of the ion are estimated. The second step is treated similarly. The total ionic potential energy is added to the energy deposited by the electrons. While their approach gives energy balance, there are some aspects of concern. The method is extremely CPU intensive, and its validity for the condensed phase is not quite evident. Considering that CK transition rates are highly sensitive to the transition energies, use of the single particle transition rates in conjunction with multivacancy configurations does not seem to be appropriate. The question of the pathways of partitioning the ionic potential energy remains unanswered. Their assumption that this energy is "locally absorbed" does not facilitate nanometric dosimetry. Because of these considerations, the low-energy electron spectrum of Pomplun *et al.*³⁰ (Table IV) is substantially different from the spectra in Tables II and III.

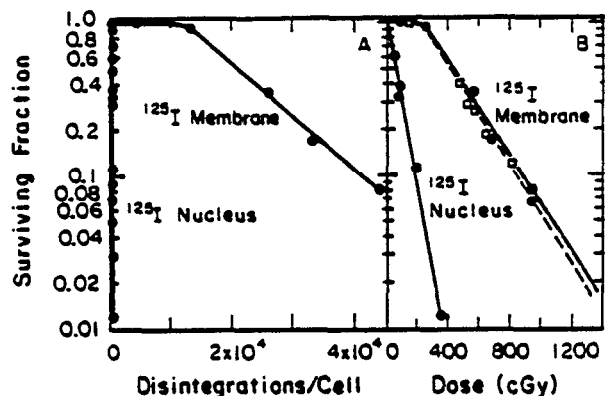


FIG. 3. Survival of Chinese hamster ovary cells: Positional effects of I-125. Note the very disparate efficacies of cell membrane bound I-125 vis-a-vis I-125 in the cell nucleus covalently incorporated into the DNA.¹⁶

(iii) The phenomenological spectrum (Table III) is derived by Sastry and Rao.³ The approach is essentially the same as that of Howell¹⁸ and Charlton and Booz.²⁸ Rather than rely totally on the theoretical rates and available tabulations of the binding energies, the experimental and theoretical results for elements in the region of $Z \approx 45$ to 55 are carefully evaluated. The calculated K and L Auger spectra are essentially the same as the experimental results reported by Casey and Albridge.³² Experimentally determined M-shell transition rates show that McGuire's theoretical level widths¹⁵ are overestimated. Accordingly, the latter are renormalized to the experimental values.³³ Perhaps the most important aspect is the failure of the independent particle model in the N shell with the onset of super CK transitions. This breakdown has been explained by Wendin and Ohno,³⁴ and Ohno³⁵ as being due to "strong dynamical effects" of collective interactions of many electrons. These effects as well as de-excitation of double-hole states are taken into account in obtaining the phenomenological spectrum³ in Table III. The major difference between this spectrum and the others is a delineation of the low energy spectrum, mostly from the N-shell transitions and entirely consistent with basic atomic physics.

III. RADIOBIOLOGICAL STUDIES

A. Experiments with cultured mammalian cells

The literature on this subject is too extensive to be included in this review. We will be concerned with studies that illustrate some aspects of interest.

1. Positional effects

Even a casual inspection of the electron spectra of I-125 (Tables II-IV) suggests that the effects of I-125 should depend on its location relative to the radiosensitive DNA in the cell nucleus. Such a dependence of the cytotoxic effects of this Auger emitter were demonstrated by Hofer and co-workers,³⁶ see Fig. 3. When in the form of ¹²⁵I-Concanavalin A, the toxicity of I-125 bound to the membrane of CHO cells is minimal and essentially the

same as for external x-rays of low LET, and sparsely ionizing β -rays from DNA-incorporated H-3 and I-131. The extremely high radiotoxicity of I-125 is manifested when it is incorporated into the DNA of proliferating cells in the chemical form of ¹²⁵IUdR, an analog of thymidine. It is important to recognize that the *chemical form* of the Auger emitter determines the subcellular localization and distribution, and the biological effects accordingly. Kassis and co-workers made important contributions to this idea using the same cell line (V79 cells), clonogenic survival being the biological end point. The relative biological effectiveness (RBE) of ¹²⁵IUdR (Ref. 37) and its analogs, ⁷⁷BrUdR (Ref. 38) and ¹²³IUdR (Ref. 39), is the same (about 7) when compared with external x-rays. ¹²⁵Iododihydrorhodamine, with ~96% of the cellular activity localized in the cytoplasm, gives RBE \approx 1.3, not very different from 1 expected for low LET radiations.⁴⁰ On the other hand, the DNA intercalator, acetamido-¹²⁵Iodoproflavine (A¹²⁵IP), gives RBE=4.8, substantially less than that for ¹²⁵IUdR. This indicates that DNA incorporation of I-125 is more effective than DNA binding.⁴¹ Furthermore, I-125 in A¹²⁵IP is several angstroms external to the DNA compared to incorporated I-125 as ¹²⁵IUdR. A more extensive discussion of these positional effects, and the experimental details may be found in Kassis *et al.*⁴² One aspect on which information is needed is the effectiveness of I-125 decay when localized in the nucleus but *not* bound to the DNA.

2. Nonuniform cytotoxicity

Although the cell nucleus, in general, is radiosensitive, the DNA is regarded as the likely molecular target. Yasui *et al.*⁴³ have shown that the toxic effects of DNA-incorporated I-125 are highly nonuniform in that the radiosensitivity depends on the region of the DNA in which ¹²⁵IUdR is incorporated. They also raise the question as to the nature of the targets, and suggest that damage to the chromatin structure, and/or higher levels of DNA organization may be of importance.⁴⁴

3. ¹²⁵IUdR vs ¹²³IUdR

As we noted earlier, the two-step decay of I-125, first by EC followed predominantly by IC, results in two equivalent Auger decay sequences. The EC decay of I-123 is followed by isomeric transitions dominated by photon emission rather than IC. Accordingly, there is essentially one Auger decay sequence associated with I-123. Makrigiorgos *et al.*³⁹ have found that for equal cell killing, I-123 decays needed are about twice as many as those of I-125. Considering that the Auger decays for the two radionuclides are approximately in the ratio of 1:2, they conclude that each one of the two steps in I-125 decay is essentially equally effective. This comparative study also re-emphasizes that localized electron irradiation of the DNA is the major cell killing mechanism rather than Coulombic molecular fragmentation. The *in vitro* studies also reveal that the radionuclides may be highly concentrated by the cells. For example, the intracellular concentration of

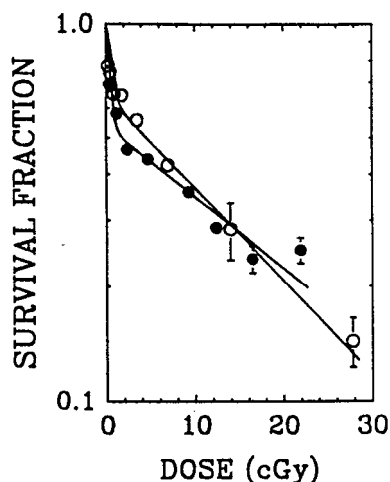


FIG. 4. *In vivo* effects of $^{125}\text{IUDR}$ (solid circles) versus those of Po-210 citrate (open circles). The Auger electrons in I-125 decay are as highly efficient as the densely ionizing 5.3-MeV alpha particles from Po-210 decay in spermatogonial cell killing.³⁷

$^{125}\text{IUDR}$ is 1800 times the concentration in the cell culture medium following incubation of V79 cells for 18 h.^{4,37} These studies have also revealed repeatedly the inadequacy of conventional dosimetry^{10,11} and the need for subcellular dosimetry in order to understand the biological effects of internal Auger emitters.^{49,45}

B. Studies in the mouse-testis model: *In vivo* effects

The *in vivo* biological effects of Auger emitters have been extensively studied by Rao *et al.* (for an overview, see Ref. 46 and references cited therein). These studies utilize spermatogenesis in mouse testes as the experimental model with spermatogonial cell killing, and induction of abnormal morphological shapes in epididymal sperm as two distinct and well-defined biological end points. The high radiosensitivity of differentiated spermatogonia (Types A₁ to A₄, In, and B) compared to the relative radioresistance of the precursor and post-gonial cells constitutes the rationale behind this model.⁴⁶⁻⁴⁸ In view of the close similarity of the biology and the radiation response between the mouse and human testes, this model is particularly relevant to humans.^{49,50}

1. Spermatogonial cell killing

Figure 4 displays results of spermatogonial cell survival studies as a function of the average testis dose for DNA-incorporated I-125 (as $^{125}\text{IUDR}$), and for Po-210 citrate. At 37% cell survival, the RBE values are 7.9 ± 2.4 and 6.7 ± 1.4 , respectively.⁵¹ Thus the *in vivo* cell killing efficacy of DNA-incorporated I-125 is as strong as that of the densely ionizing 5.3 MeV high LET alpha particles from Po-210 decay. The compound, HIPDM, is a brain perfusion imaging agent when labeled with I-123. It is found that $\text{H}^{125}\text{IPDM}$ localizes in the cytoplasm of the testicular cells only. The RBE value for this agent is 1.0.⁵² This positional dependence of RBE of the Auger emitter on its subcellular localization, governed by the chemical form, re-emphasizes

the earlier findings of Rao *et al.* with In-111 oxine and In-111 citrate,⁵³ and establishes the concept of positional effects *in vivo* much like with cells in culture.^{36,42} The emergence of this principle in spite of the complexities of *in vivo* systems is an important contribution indeed. With $^{125}\text{IUDR}$ and $\text{H}^{125}\text{IPDM}$ setting the extremes of subcellular localization (DNA versus cytoplasm), it is possible to examine the dependence of RBE on the DNA-bound fraction of I-125 when the Auger emitter is localized in the testicular cells in *both* chemical forms. Using binary mixtures of the two I-125 labeled agents, Howell *et al.*⁵⁴ have found a linear relation between RBE and f_d , the ratio of DNA-incorporated I-125 activity in the testicular cells to the total I-125 activity in the organ: $\text{RBE} = 1.0 + 7.4 f_d$, with $f_d \leq 1.0$. It appears that the contributions of low-LET radiations are represented by the intercept while the slope may be related to high-LET effects. Such quantitative results of *in vivo* radiobiological studies hold the promise that chemical form, subcellular distribution and microdosimetry of the Auger emitter might be combined into one single equation. It would be worthwhile that this approach is extended to cases where I-125 is localized in other cellular compartments such as the nucleus (without binding to DNA), and the chromatin.

2. Abnormal sperm shapes

At the end of the spermatogenesis, the mouse sperm have characteristic hooklike head shapes. These spermatozoa migrate through the tubules, and they are stored in the epididymis, a small saclike structure adjacent to the testis. Sperm shape abnormalities of head, stem, and tail are known.⁵⁵ Even in normal mice, a small (2%-3%) fraction of epididymal sperm have abnormal shapes. A variety of agents (radiation, chemicals, etc.) can cause elevated levels of abnormal sperm over the remarkably constant spontaneous value. Rao *et al.*⁴⁶ have found that Auger emitters are very effective in inducing such shape abnormalities at *extremely low doses* to the organ, the efficacies depending again on the chemical form and subcellular distribution of the Auger emitter. Internal β emitters and external x-rays are only marginally effective. Figure 5 shows the results for $^{125}\text{IUDR}$ and Po-210 citrate α -particles. The sharp initial rise followed by a saturation at higher doses is a characteristic feature of the dose-response curves. The relevant parameter for intercomparison is the initial slope. RBE values, derived in comparison with the initial slope of the curve for 120 kVp external x-rays, are about 250 and 60 for Po-210 citrate and $^{125}\text{IUDR}$, respectively. Extensive results and details are given by Rao *et al.*⁵⁶ on studies involving this biological effect. Three aspects are noted here. First, abnormal sperm shape induction is a very sensitive biological monitor of the *in vivo* effects of internal Auger and α emitters. Second, although the RBE values for cell killing are essentially the same for $^{125}\text{IUDR}$ and Po-210 citrate, the α emitter is definitely more effective in inducing abnormal sperm shapes. This is quite reasonable when one considers the fact that the high-LET 5.3 MeV α rays, with a range of 5-6 cell diameters, can hit more cells and cause subtle but nonlethal damage whereas the simulated high-LET effects

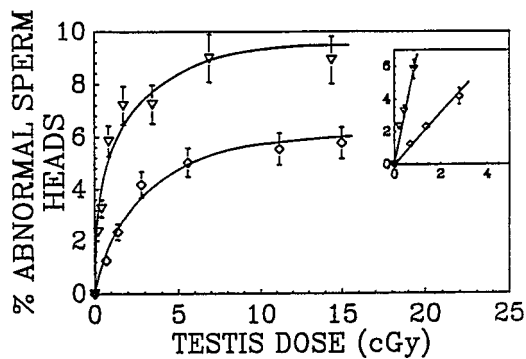


FIG. 5. Comparison of DNA-bound I-125 with an emitter (Po-210 citrate) in causing abnormalities in sperm shape. The percentage of abnormal epididymal sperm is shown as a function of the testicular absorbed dose for $^{125}\text{IuDR}$ (open diamonds) and ^{210}Po -citrate (inverse open triangles). Error bars represent the standard error. An enlargement of the low dose region of the curve is illustrated in the upper right corner. The efficacy of these radiochemicals in inducing abnormalities at very low doses is indicated by the large initial slopes. Based on the initial slopes, the particles emitted by ^{210}Po are about 4 times more effective in producing sperm abnormalities than the dense shower of Auger electrons emitted by DNA-bound I-125. The vertical scale represents the excess abnormal fraction over the spontaneous value.⁵⁶ See text for added remarks.

of $^{125}\text{IuDR}$ are limited to the target cell itself. Third, the RBE values for both the biological end points show a linear relationship: $\text{RBE}_A = 8.8 (\text{RBE}_S) - 5.3$, where $A = \text{abnormal}$ and $S = \text{survival}$, the only exception to this being the results for the alpha emitter.

3. Mechanisms of radiation action and chemical protectors

Radioprotection by chemicals such as cysteamine (MEA), ascorbic acid, WR-2721, etc. against external low-LET radiations are well known, both *in vitro* and *in vivo*. Very little is known concerning chemical protection against the chronic irradiation effects of incorporated radionuclides. The protective action is generally denoted by the dose modification factor ($\text{DMF} = \text{mean lethal dose with the chemical} / \text{mean lethal dose without the chemical}$). $\text{DMF} > 1$ implies protection. Data in Fig. 6 reveal interesting new results.⁵² When mouse testes are pretreated with very small and nontoxic amounts (0.75 μg) of MEA per

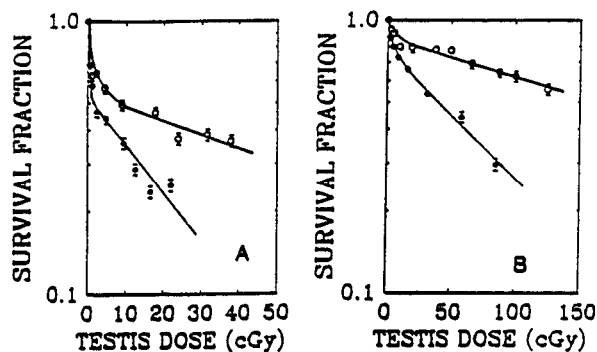


FIG. 6. Spermatogonial cell survival in the presence of MEA (open circles) and in its absence (solid circles): (a) $^{125}\text{IuDR}$; (b) $\text{H}^{125}\text{IPDM}$.⁵²

mouse, the severe high-LET type cytotoxic effects of $^{125}\text{IuDR}$ [Fig. 6(a)] as well as the low-LET-type effects of cytoplasmic ^{125}I as $\text{H}^{125}\text{IPDM}$ [Fig. 6(b)] are strongly mitigated. The respective DMFs are 3.6 ± 1.1 and 3.8 ± 0.6 . The results are highly reproducible. For Po-210 citrate, $\text{DMF} = 2.6 \pm 0.5$. Comparable results are obtained with L-ascorbic acid as well: $\text{DMF} \sim 2.2$, Rao.⁵⁷ Abnormal sperm assay also shows a drastic reduction in the initial slopes by a factor of 14 with $^{125}\text{IuDR}$, and 10 with Po-210 citrate⁵⁶ in the presence of MEA.

The above results are quite unexpected and entirely new, with a potential for a major impact on the hitherto unexplored area of incorporated radionuclides and protectors. Much work is needed to answer a number of questions that arise concerning the complex mechanisms of protective action.⁵⁸ Of particular interest to our discussion are the implications of the above results to the mechanisms of action of Auger emitters. What is the primary mechanism: direct or indirect? The former, involving direct energy deposition in the sensitive targets, is generally believed to be the initial mechanism of high-LET-type damage by a particles⁵⁹ and DNA-incorporated I-125.^{3,37,60,61} Large DMFs are not expected for direct action,⁵⁹ although Bird⁶² reported results to the contrary. On the other hand, the damage by low-LET radiations involves primarily the indirect action via secondary interactions between the DNA and the highly reactive free radicals (e.g., $\text{OH}\cdot$) produced in the radiolysis of water. Inasmuch as damage by free radicals can be prevented by scavenging molecules, large DMFs are expected in this case. The result for $\text{H}^{125}\text{IPDM}$ (in the cytoplasm) is consistent with the accepted phenomenology of radiobiology. What is surprising here is the large DMF for $^{125}\text{IuDR}$ as well as Po-210 citrate. If one concedes that free radical scavenging is one of the primary mechanisms of chemical radioprotection, the results of Rao *et al.*^{52,56} imply a major role for the indirect effect. Track structure calculations⁶³ do reveal (see below) a preponderance of OH^* radicals in the close proximity of the DNA. Thus the question of direct versus indirect action is wide open. Moreover, what are the targets (e.g., the entire DNA, nucleosomes, chromatin, nucleoproteins), and where are they located?^{43,44} If they are just on the inside of the nuclear membrane as surmised by Cole,⁶⁴ the dose rate profile (Fig. 7) for I-125 in the cytoplasm and in the nucleus suggests that $\text{H}^{125}\text{IPDM}$ must be much more toxic than the *in vivo* findings.⁵²

IV. DOSIMETRY OF I-125

A. Conventional dosimetry

The MIRD Schema and ICRU procedures^{10,11} are used with the assumption that the radionuclide and the radiation energy are uniformly distributed in the organ. Low-energy electrons from Auger emitters contribute negligibly to the macroscopic dose, and their potential for localized damage is ignored. This approach does not consider either the chemical form and subcellular distribution of the Auger emitter, or the possibility that the radionuclide may be concentrated by the cells. The cellular geom-

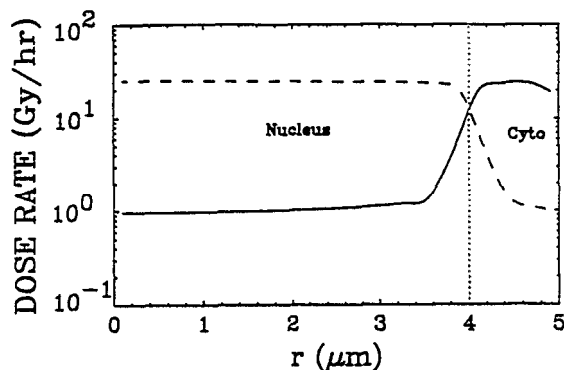


FIG. 7. Relative dose rate profiles for I-125 in the nucleus, and in the cytoplasm distributed uniformly in either of the cellular regions. The nucleus and the cells are assumed to be concentric spheres of radius 4 and 5 μm , respectively. The radial coordinate (r) is measured from the center of the nucleus. The solid (dashed) curve is for I-125 in the nucleus (cytoplasm) of the cell.⁵²

etry and the packing of cells in the organ are ignored. These are some of the reasons for the inadequacy of conventional dosimetry. Both *in vitro* and *in vivo* studies have amply drawn attention to this aspect,^{45,47} and pointed out the need for subcellular dosimetry of internal Auger emitters.

B. Subcellular dosimetry

Sastry and co-workers developed approaches to cellular dosimetry by explicitly taking account of the limitations of conventional dosimetry in a phenomenological manner.^{3,4} Nuclear dose enhancement factors derived in this context adequately account for the positional effects of Auger emitters *in vitro* and *in vivo*. Specific expressions may be found in Ref. 4, for example.

C. Localized pattern of energy deposition

Figure 8 shows the localized pattern of energy deposition around the decay site of I-125 in tissue equivalent matter. The phenomenological spectrum³ in Table III and the data in Table I are used along with Cole's data on energy-range relations for electrons.²³ The changing LET of the electrons is considered in the continuously slowing down approximation (csda). See Refs. 29 and 65 for calculational methods. Results obtained with Monte Carlo methods are in good agreement, and show considerable overestimation in the csda approach only at distances ≤ 2 nm from the decay site.⁴

D. Calculation of DNA strand breaks

Charlton⁶⁶ and Charlton and Humm⁶⁷ modeled the DNA and calculated, using Monte Carlo codes, the distributions of energy depositions at the sub-nanometric and nanometric level by Auger electrons from I-125 decay located in the middle of the double helix. They also calculated the initial damage in terms of single and double strand breaks. Their results account for the frequency distribution of the positions of strand breaks from the site of

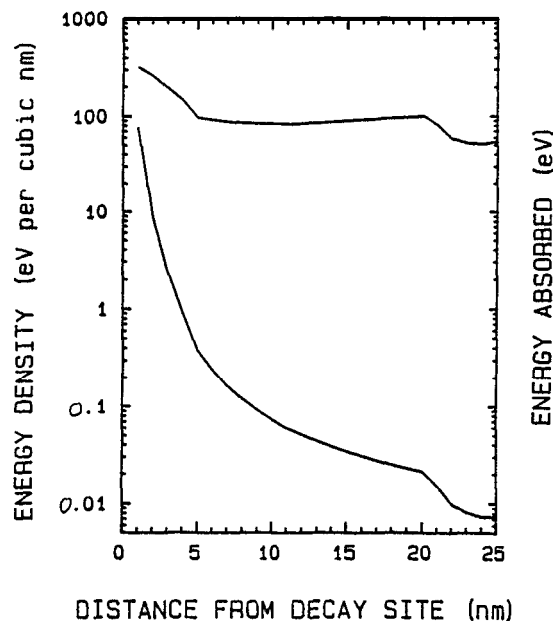


FIG. 8. Localized energy deposition around I-125 decay site. The pattern of average energy deposited by the Auger and CK electrons is shown by the top curve. The value at 1 nm is the energy absorbed in a unit density sphere of this radius, centered at the decay site. Energy deposited in 1-nm-thick concentric spherical shells thereafter is indicated as a function of the distance from the decay site. The discontinuities at about 5 and 20 nm are due to the end of the range of major low-energy electron groups. The lower curve, derived from the top one, is the profile of the average absorbed energy density. The sharp drop in the energy density in the first 5 nm illustrates the highly localized nature of the action of the low-energy electrons.³⁷ Note that 10 eV/(nm³) implies a locally absorbed dose of 1.6 MGy.

I-125 incorporation, originally reported by Martin and Haseltine.⁶⁸ See Figure 9 and Refs. 66-68 for more details.

E. Track structure calculations

Wright *et al.*⁶³ performed track structure calculations in liquid water for Auger emitters and for 4.0 and 5.3 MeV alpha particles using Monte Carlo methods and the Oak Ridge Electron Transport Code and Radiolysis Code.

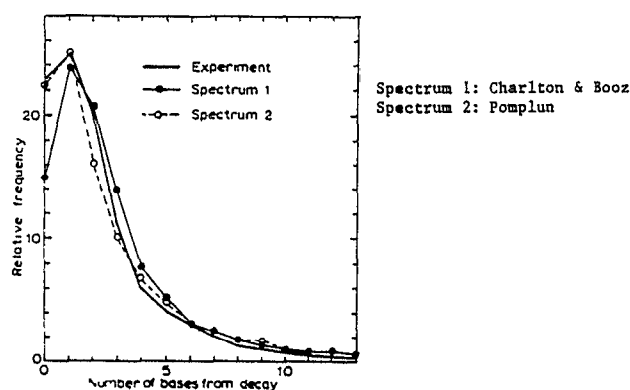


FIG. 9. Calculations of Charlton and Humm and explanation of the DNA single strand breaks observed by Martin and Haseltine.^{67,68} Shown in the figure is the relative frequency of strand breaks versus distance (number of bases) from the site of decay.

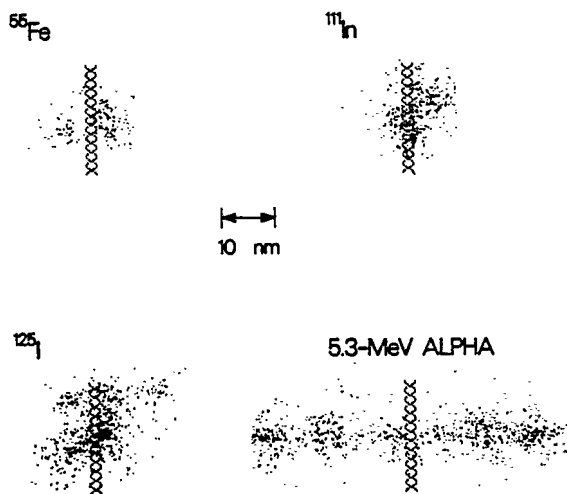


FIG. 10. Initial positions of the reactive chemical species (e.g., OH \cdot , H \cdot , e $^-_{aq}$, etc.) for different Auger emitters. The emitter is located at the midpoint on the surface of a cylindrical DNA segment in liquid water.⁶³

Both direct and indirect interactions with the DNA are scored, and the spatial and temporal patterns of the reactive species are followed (10^{-12} s to 10^{-6} s). Figure 10 shows an example of the distribution of chemical species for some Auger emitters at $t = 10^{-12}$ s. The species density is large for I-125; and for all the Auger emitters, the density is at least as high or larger than along the track of the α particles.^{49,63} The spatial distribution of the various reactive species is presented in Figure 11 for I-125. The largest fraction consists of the OH \cdot radicals which are implicated in chemical damage of the DNA strands. These interesting initial results suggest that the indirect effect may indeed be an important mechanism. They also permit calculations of interactions with radical scavengers and chemical protectors.

V. DISCUSSION AND CONCLUSION

This review of Iodine-125 data is presented to the scientific community through the AAPM Task Group No. 6. Constraints of space did not permit as much elaboration as

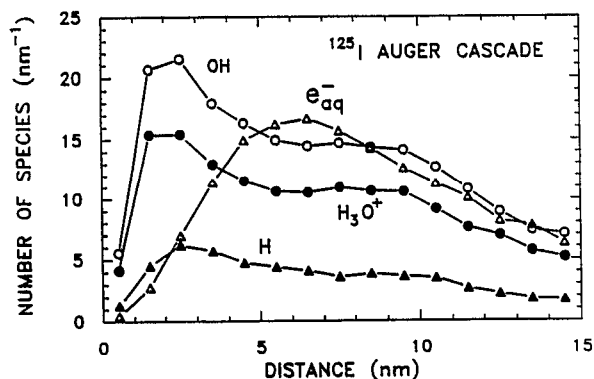


FIG. 11. Initial number of chemical species in 1-nm-thick spherical shells centered on the Auger emitter I-125.⁶³

some of the areas might have warranted. The numerous studies on bacterial systems and microorganisms are not included for the same reason. Nevertheless, most of the aspects relevant to mammalian cells are brought to the attention of the interested reader. The literature cited, though necessarily not complete, should be adequate for a further examination of the field. All experimental data to date confirm the high radiotoxicity of DNA-incorporated I-125 in a number of biological end points both *in vitro* and *in vivo*. Recent work of Kassis *et al.*⁶⁹ with ^{125}I UdR and ^{125}I UdR introduced directly into rat brain tumors points to diagnostic (^{125}I UdR) and therapeutic implications (^{125}I UdR) in humans. Bagshawe and colleagues^{70,71} are exploring the clinical potential of selective uptake of ^{125}I UdR by resistant tumors.

Besides I-125, *in vitro* studies⁴² and *in vivo* studies^{46,56} with a variety of radiochemicals labeled with Auger emitters widely used in Nuclear Medicine have revealed radiotoxic effects considerably greater than expectations based on conventional dosimetry. These as well as the radiobiological studies with I-125 provide a compelling rationale for the scientific community to arrive at biophysically meaningful ways of estimating the risks of Auger emitters of interest to diagnosis and therapy. The theoretical and experimental data with I-125 reviewed here should provide sufficient guidance in this endeavor. A number of questions need to be addressed in this context. What are the radiosensitive targets and what are the nonrepairable critical lesions? Is localized energy deposition in the DNA the primary mechanism of damage? If so, how should the Auger electron spectra be calculated in a way relevant to matter in the condensed phase? Is microdosimetry an adequate approach if a considerable amount of energy is locked up as potential energy of the residual ion?³⁰ How is such energy redistributed? What other mechanisms are likely to be of importance: long-range charge and energy migration along the DNA,⁷² super-excited states,⁷³ etc.? What is the relative importance of direct and indirect action of radiation? What is the role of chemical agents that may modulate the initial damage?

The above questions are not necessarily exhaustive. It may not be prudent, however, to await answers to all of them. One thing is clear. The interdisciplinary science of I-125 has been exciting, and future studies may well be expected to shed important new light. This optimism is strongly based on the scientific presentations⁷⁴ and intensive interactions between the participants of the Second International Symposium on Biophysical Aspects of Auger Processes held at the University of Massachusetts/Amherst, 5-6 July 1991. While we await publication of the Proceedings of the Symposium, suffice it to note that a number of the questions raised above have been examined incisively. These emerging insights along with the understanding already on hand are adequate to make a beginning to consider plausible ways toward obtaining reasonably realistic estimates of the effects of internal Auger emitters *in vivo*.

ACKNOWLEDGMENTS

This work is supported by USPHS Grant No. CA32877. Special thanks are due to Mrs. Doris Atkins for her assistance.

- ⁴James G. Kereiakes, Co-Chairman, Dandamudi V. Rao, Co-Chairman, Roger W. Howell, John L. Humm, Ravinder Nath, Kanduia S. R. Sastry, Sven-Erik Strand, and Stephen R. Thomas.
- ⁵W. Bambynek, B. Crasemann, R. W. Fink, R.-U. Freund, H. Mark, C. D. Swift, R. E. Price, and P. Venugopala Rao, "X-ray fluorescence yields, Auger and Coster-Kronig transition probabilities," *Rev. Mod. Phys.* 44, 716-813 (1972).
- ⁶E. J. McGuire, "Auger and Coster-Kronig transitions," in *Atomic Inner-Shell Processes, Vol. I: Ionization and Transition Probabilities*, edited by B. Crasemann (Academic, New York, 1975), pp. 293-330.
- ⁷K. S. R. Sastry and D. V. Rao, "Dosimetry of low energy electrons," in *Physics of Nuclear Medicine: Recent Advances*, edited by D. V. Rao, R. Chandra, and M. Graham (AAPM, Medical Physics Monograph No. 10, American Institute of Physics, 1984), pp. 169-208.
- ⁸K. S. R. Sastry, R. W. Howell, D. V. Rao, V. B. Mylavarapu, A. I. Kassis, S. J. Adelstein, H. A. Wright, R. N. Hamm, and J. E. Turner, "Dosimetry of Auger emitters: Physical and phenomenological approaches," in *DNA Damage by Auger Emitters*, edited by K. F. Baverstock and D. E. Charlton (Taylor & Francis, London, 1988), pp. 27-38.
- ⁹See, for example, E. H. S. Burhop. *The Auger Effect and Other Radiationless Transitions* (Cambridge U. P., Cambridge, 1952), Plates I and II.
- ¹⁰M. E. Wrenn, "Dosimetry of ⁵⁵Fe," International Radiation Protection Association: Symposium Proceedings, Rome, 1966, pp. 843-850.
- ¹¹Auger cascades and nuclear medicine: Editorial. *The Lancet* Vol. II:533-534 (1985).
- ¹²K. S. R. Sastry and D. V. Rao, "Biological damage caused by Auger cascades," *The Lancet* Vol. I, 858-859 (1986).
- ¹³D. V. Rao and K. S. R. Sastry, "Radiobiological effects of Auger emitters *in vitro* and *in vivo*," in *Radiation Research: Vol. 2*, edited by E. M. Fielden, J. F. Fowler, J. H. Hendry, and D. Scott, Proc. 8th ICRP, Edinburgh, 1987 (Taylor & Francis, London, 1988), pp. 369-374.
- ¹⁴R. Loevinger and M. Berman, *A Rev&d Schema for Calculating the Absorbed Dose from Biologically Distributed Radionuclides*, MIRD Pamphlet No. 1, revised (The Society of Nuclear Medicine, New York, March, 1976).
- ¹⁵ICRU Report 32, "Methods of assessment of absorbed dose in clinical use of radionuclides," International Commission on Radiation Units and Measurements, Washington, DC (1979).
- ¹⁶See, for example, M. J. Martin and P. J. Blichert-Toft. "Radioactive atoms, Auger-electron, α -, β -, γ -, and X-ray data," *Nucl. Data Tables A8*, 1-198 (1970).
- ¹⁷M. H. Chen, B. Crasemann, and H. Mark, "Relativistic radiationless transition probabilities for atomic K- and L-shells," *Atomic Data Nucl. Data Tables* 24, 13-37 (1979).
- ¹⁸F. P. Larkins, "Semi-empirical Auger electron energies for elements $10 \leq Z \leq 100$," *Atomic Data Nucl. Data Tables* 20, 311-387 (1977).
- ¹⁹E. J. McGuire, *M-shell Auger, Coster-Kronig, and Radiative Matrix Elements, and Auger and Coster-Kronig Transition Rates in j-j Coupling*, Research Report SC-RR-710835, Sandia Laboratories, 1972. (Available from National Technical Information Service, Springfield, VA 22161).
- ²⁰E. J. McGuire, *N-Shell Auger, Coster-Kronig, and Radiative Matrix Elements, and Auger and Coster-Kronig Transition Rates in j-j Coupling*, Report SAND-75-0043, Sandia Laboratories, 1975. (Available from National Technical Information Service, Springfield, VA 22161).
- ²¹M. F. Chung and L. H. Jenkins, "Auger electron energies of the outer shell electrons," *Surf. Sci.* 22, 479-485 (1970).
- ²²R. W. Howell, "Radiation spectra for Auger-electron emitting radionuclides," Report No. 2 of AAPM Nuclear Medicine Task Group No. 6, *Med. Phys.* 19, xxx-xxx (1992).
- ²³K. D. Sevier, *Low Energy Electron Spectrometry* (Wiley-Interscience, New York, 1972) pp. 356-373.
- ²⁴J. A. Bearden and A. F. Burr, "Re-evaluation of X-ray atomic energy levels," *Rev. Mod. Phys.* 39, 125-142 (1967).
- ²⁵T. A. Carlson and R. M. White, "Formation of fragment ions from $\text{CH}_3^{125}\text{Te}$ and $\text{C}_2\text{H}_5^{125}\text{Te}$ following the nuclear decays of $\text{CH}_3^{125}\text{I}$ and $\text{C}_2\text{H}_5^{125}\text{I}$," *J. Chem. Phys.* 38, 2930-2934 (1963).
- ²⁶E. Storm and H. I. Israel, "Photon cross sections from 1 keV to 100 MeV for elements $Z = 1$ to 100," *Nucl. Data Tables A8*, 1-198 (1970).
- ²⁷A. Cole, "Absorption of 20-eV to 50,000 eV electron beams in air and plastic," *Radiat. Res.* 38, 7-33 (1969).
- ²⁸R. Deutzmann and G. Stöcklin, "Chemical effects of I-125 decay in aqueous solution of 5-Iodouracil: Ring fragmentation as a consequence of the Auger effect," *Radiat. Res.* 87, 24-36 (1981).
- ²⁹U. Linz and G. Stöcklin, "Chemical and biological consequences of the radioactive decay of Iodine-125 in plasmid DNA," *Radiat. Res.* 101, 262-278 (1985).
- ³⁰M. L. Knotek and P. J. Feibelman, "Ion desorption by core-hole Auger decay," *Phys. Rev. Lett.* 40, 964-967 (1978).
- ³¹M. L. Knotek, V. O. Jones, and V. Rehn, "Photon stimulated desorption of ions," *Phys. Rev. Lett.* 43, 300-303 (1979).
- ³²D. E. Charlton and J. Booz, "A Monte Carlo treatment of the decay of ^{125}I ," *Radiat. Res.* 87, 10-23 (1981).
- ³³R. W. Howell, K. S. R. Sastry, H. Z. Hill, and D. V. Rao, "Cis-Platinum-193m: Its microdosimetry and potential for chemo-Augur combination therapy of cancer," in *Proc. 4th International Radiopharmaceutical Dosimetry Symposium*, edited by A. T. Schläfke-Stelson and E. E. Watson (Dept. of Energy, Oak Ridge, TN, 1986), CONF 85-1113, pp. 493-513.
- ³⁴E. Pomplun, J. Booz, and D. E. Charlton, "A Monte Carlo simulation of Auger cascades," *Radiat. Res.* 111, 533-552 (1987).
- ³⁵J. P. Desclaux, "A multi-configuration relativistic Dirac-Fock program," *Comput. Phys. Commun.* 9, 31-45 (1975).
- ³⁶W. R. Casey and R. G. Albridge, "The L and K Auger spectra of tellurium," *Z. Phys.* 219, 216-226 (1969).
- ³⁷S. Svensson, N. Martensson, E. Basilier, P. Malmquist, U. Gelius, and K. Siegbahn, "Lifetime broadening and CI-resonances observed in ESCA," *Phys. Scr.* 14, 141-147 (1976).
- ³⁸G. Wendin and M. Ohno, "Strong dynamical effects of many-electron interactions in photoelectron spectra from 4s and 4p core levels," *Phys. Scr.* 14, 148-161 (1976).
- ³⁹M. Ohno, "Strong dynamical effects in the X-ray photoemission spectra and X-ray emission spectra of the elements Pd to Xe," *Phys. Scr.* 21, 589-593 (1980).
- ⁴⁰K. G. Hofer, "Toxicity of radionuclides as a function of subcellular dose distribution," in *Third International Radiopharmaceutical Dosimetry Symposium*, edited by E. E. Watson, A. T. Schläfke-Stelson, J. L. Coffey, and J. Cloutier (US Department of Health & Human Services, 1981) HHS Publication FDA 81-8166, pp. 371-391 (Also see references cited therein).
- ⁴¹A. I. Kassis, S. J. Adelstein, and K. S. R. Sastry, "Kinetics of uptake, retention and radiotoxicity of ^{125}I UdR in mammalian cells: Implications of localized energy deposition by Auger processes," *Radiat. Res.* 109, 78-89 (1987).
- ⁴²A. I. Kassis, S. J. Adelstein, C. Haydock, K. S. R. Sastry, K. D. McElvany, and M. J. Welch, "Lethality of Auger electrons from the decay of Bromine-77 in the DNA of mammalian cells," *Radiat. Res.* 90, 362-373 (1982).
- ⁴³G. M. Makrigiorgos, A. I. Kassis, J. Baranowska-Kortylewicz, K. D. McElvany, M. J. Welch, K. S. R. Sastry, and S. J. Adelstein, "Radiotoxicity of 5-[I-123]Iodo-2'-deoxyuridine in V79 cells: A comparison with 5-[I-125]Iodo-2'-deoxyuridine," *Radiat. Res.* 118, 532-544 (1989).
- ⁴⁴A. I. Kassis, F. Fayad, B. M. Kinsey, K. S. R. Sastry, R. A. Taube, and S. J. Adelstein, "Radiotoxicity of I-125 in mammalian cells," *Radiat. Res.* 111, 305-318 (1987).
- ⁴⁵A. I. Kassis, F. Fayad, B. M. Kinsey, K. S. R. Sastry, and S. J. Adelstein, "Radiotoxicity of an I-125 labeled DNA intercalator in mammalian cells," *Radiat. Res.* 118, 283-294 (1989).
- ⁴⁶A. I. Kassis, S. J. Adelstein, R. W. Howell, and K. S. R. Sastry, "Positional effects of Auger decays in mammalian cells in culture," in *DNA Damage by Auger Emitters*, edited by K. F. Baverstock and D. E. Charlton (Taylor & Francis, London, 1988), pp. 1-13.
- ⁴⁷L. S. Yasui, K. G. Hofer, and R. L. Wartens, "Inhomogeneity of the nucleus to ^{125}I UdR cytotoxicity," *Radiat. Res.* 102, 106-118 (1985).
- ⁴⁸L. S. Yasui, R. L. Wartens, A. S. Paschoa, and K. G. Hofer, "Cytotoxicity of I-125 decay-produced lesions in chromatin," in *DNA Damage by Auger Emitters* edited by K. F. Baverstock and D. E. Charlton (Taylor & Francis, London, 1988), pp. 181-189.

- ⁴⁵S. J. Adelstein, A. I. Kassis, and K. S. R. Sastry, "Cellular vs. organ approaches to dose estimates," in *Proc. 4th International Radiopharmaceutical Dosimetry Symposium*, edited by A. T. Schläpke-Stelson and E. E. Watson (Dept. of Energy, Oak Ridge, TN, 1986), CONF 85-1113, pp. 13-25.
- ⁴⁶D. V. Rao, V. B. Mylavarapu, K. S. R. Sastry, and R. W. Howell, "Internal Auger emitters: Effects on spermatogenesis and oogenesis in mice," in *DNA Damage by Auger Emitters*, edited by K. F. Baverstock and D. E. Charlton (Taylor & Francis, London, 1988) pp. 15-26.
- ⁴⁷D. V. Rao, G. F. Govelitz, and K. S. R. Sastry, "Radiotoxicity of Thallium-201 in mouse testes: Inadequacy of conventional dosimetry," *J. Nucl. Med.* 24, 145-153 (1983).
- ⁴⁸M. L. Meistrich, N. R. Hunter, N. Suzuki, P. K. Trostle, and H. R. Withers, "Gradual regeneration of mouse testicular stem cells after exposure to ionizing radiation," *Radiat. Res.* 74, 349-362 (1978).
- ⁴⁹M. L. Meistrich and R. C. Samuels, "Reduction in sperm levels after testicular irradiation of the mouse: A comparison with man," *Radiat. Res.* 102, 138-147 (1985).
- ⁵⁰M. E. Gauden, "'Biological dosimetry' of radionuclides and radiation hazards," *J. Nucl. Med.* 24, 160-164 (1983).
- ⁵¹D. V. Rao, V. R. Narra, R. W. Howell, G. F. Govelitz, and K. S. R. Sastry, "In vivo radiotoxicity of DNA-incorporated I-125 compared with that of densely ionising alpha-particles," *The Lancet* Vol. II, No. 8664, 650-652 (1989).
- ⁵²D. V. Rao, V. R. Narra, R. W. Howell, and K. S. R. Sastry, "Biological consequence of nuclear versus cytoplasmic decays of I-125: Cysteamine as a radioprotector against Auger cascades in vivo," *Radiat. Res.* 124, 188-193 (1990).
- ⁵³D. V. Rao, K. S. R. Sastry, H. E. Grimmond, R. W. Howell, G. F. Govelitz, V. K. Lanka, and V. B. Mylavarapu, "Cytotoxicity of some indium radiopharmaceuticals in mouse testes," *J. Nucl. Med.* 29, 375-384 (1988).
- ⁵⁴R. W. Howell, D. V. Rao, D-Y. Hou, V. R. Narra, and K. S. R. Sastry, "The question of RBE and quality factor for Auger emitters incorporated into proliferating mammalian cells," *Radiat. Res.* 128, 282-293 (1991).
- ⁵⁵A. J. Wyrobek, "Changes in mammalian sperm morphology after x-ray and chemical exposure," *Genetics* 92, S105-S119 (1979).
- ⁵⁶D. V. Rao, V. R. Narra, R. W. Howell, V. K. Lanka, and K. S. R. Sastry, "Induction of spermhead abnormalities by incorporated radionuclides: Dependence on subcellular distribution, type of radiation, dose rate, and presence of radioprotectors," *Radiat. Res.* 125, 89-97 (1991).
- ⁵⁷D. V. Rao (personal communication, 1991).
- ⁵⁸J. C. Livesey and D. J. Reed, "Chemical protection against ionizing radiation," *Adv. Radiat. Biol.* 13, 285-339 (1987).
- ⁵⁹G. W. Barendsen and H. M. D. Walter, "Effects of different ionizing radiations on human cells in tissue culture. IV. Modification of radiation damage," *Radiat. Res.* 21, 314-329 (1964).
- ⁶⁰D. E. Charlton, "The range of high LET effects from I-125 decays," *Radiat. Res.* 107, 163-171 (1986).
- ⁶¹K. G. Hofer, G. Keough, and J. M. Smith, "Biological toxicity of Auger emitters: Molecular fragmentation versus electron irradiation," *Curr. Top. Radiat. Res. Q* 12, 335-354 (1977).
- ⁶²R. P. Bird, "Cysteamine as a protective agent with high LET radiations," *Radiat. Res.* 82, 290-296 (1980).
- ⁶³H. A. Wright, R. N. Hamm, J. E. Turner, R. W. Howell, D. V. Rao, and K. S. R. Sastry, "Calculations of physical and chemical reactions with DNA in aqueous solutions from Auger cascades," *Radiat. Prot. Dosim.* 31, 59-62 (1990).
- ⁶⁴A. Cole, W. G. Cooper, F. Shonka, P. M. Corry, R. M. Humphrey, and A. T. Ansevin, "DNA scission in hamster cells and isolated nuclei studied by low-voltage electron beam irradiation," *Radiat. Res.* 60, 1-33 (1974).
- ⁶⁵A. I. Kassis, S. J. Adelstein, C. Haydock, and K. S. R. Sastry, "Radiotoxicity of Se-75 and S-35: Theory and application to a cellular model," *Radiat. Res.* 84, 407-425 (1980).
- ⁶⁶D. E. Charlton, "Calculation of single strand and double strand DNA breakage from incorporated I-125," in *DNA Damage by Auger Emitters*, edited by K. F. Baverstock and D. E. Charlton (Taylor & Francis, London, 1988), pp. 89-100.
- ⁶⁷D. E. Charlton and J. L. Humm, "A method of calculating initial DNA strand breakage following the decay of incorporated I-125," *Int. J. Radiat. Biol.* 53, 353-365 (1988).
- ⁶⁸R. F. Martin and W. A. Haseltine, "Range of radiochemical damage to DNA with decay of iodine-125," *Science* 213, 896-898 (1981).
- ⁶⁹A. I. Kassis, A. D. Van den Abbeele, P. Y. Wen, J. Baranowska-Kortylewicz, R. A. Aaronson, W. C. DeSisto, L. A. Lampson, P. M. Black, and S. J. Adelstein, "Specific uptake of the Auger electron-emitting thymidine analogue 5-[I-123/I-125] Iodo-2'-deoxyuridine in rat brain tumors: Diagnostic and therapeutic implications in humans," *Cancer Res.* 50, 5199-5203 (1990).
- ⁷⁰K. D. Bagshawe, S. K. Sharma, P. J. Southal, J. A. Boden, G. M. Boxer, T. A. Patridge, P. Antoniwi, and R. B. Pedley, "Selective uptake of toxic nucleoside (¹²⁵IUdR) by resistant cancer," *Br. J. Radiol.* 64, 37-44 (1991).
- ⁷¹J. L. Humm, K. D. Bagshawe, S. K. Sharma, and G. Boxer, "Tissue dose estimates following the selective uptake of ¹²⁵IUdR and other radiolabeled thymidine precursors in resistant tumors," *Br. J. Radiol.* 64, 45-49 (1991).
- ⁷²K. F. Baverstock and R. B. Cundall, "Solitons and energy transfer in DNA," *Nature* 332, 312-313 (1988).
- ⁷³A. Halpern, "Intra- and intermolecular energy transfer and superexcitation in post-Auger processes," *Radiochimica Acta* 50, 129-134 (1990).
- ⁷⁴K. G. Hofer, "Symposium Report: Biophysical aspects of Auger processes," *Int. J. Radiat. Biol.* 61, 289-292 (1992).

Radiation spectra for Auger-electron emitting radionuclides: Report No. 2 of AAPM Nuclear Medicine Task Group No. 6^{a)}

Roger W. Howell

Department of Radiology, University of Medicine & Dentistry of New Jersey, New Jersey Medical School,
185 S. Orange Avenue, Newark, New Jersey 07103

(Received 16 March 1992; accepted for publication 22 April 1992)

Radiation spectra for radionuclides currently provided by the MIRD Committee and ICRP do not include the very low-energy N- and O-shell Auger electrons. These electrons, emitted in large numbers by radionuclides decaying by electron capture and/or internal conversion, are important for determining the absorbed dose in microscopic volumes. Accordingly, the present AAPM Report employs Monte Carlo computational methods to obtain a self-consistent set of complete radiation spectra for a variety of radionuclides including ^{55}Fe , ^{67}Ga , $^{99\text{m}}\text{Tc}$, ^{111}In , $^{113\text{m}}\text{In}$, $^{115\text{m}}\text{In}$, ^{123}I , ^{125}I , $^{193\text{m}}\text{Pt}$, $^{195\text{m}}\text{Pt}$, ^{201}Tl , and ^{203}Pb . Although the conventional spectra provided by MIRD and ICRP are adequate for most dosimetry calculations, the Auger electron spectra provided in this report are recommended for calculating the dose to target volumes $< 1 \mu\text{m}$ in diameter.

I. INTRODUCTION

A. Scope

A wide variety of radionuclides are used in diagnostic and therapeutic Nuclear Medicine. Many of the photon emitters commonly utilized for diagnostic imaging are radionuclides that decay by electron capture (EC) or internal conversion (IC). Examples of such radionuclides include ^{67}Ga , $^{99\text{m}}\text{Tc}$, ^{111}In , ^{123}I , and ^{201}Tl . In addition to diagnostically useful photons, these radionuclides emit numerous low-energy Auger electrons through a complex series of atomic processes. The extreme radiotoxicity of Auger-electron emitters is well established^{1,2,3,4,9} and is attributed to the highly localized energy deposition (HILED) in the immediate vicinity of the decay site.^{1,2,4-9} Conventional organ dosimetry,^{10,11} which ignores HILED, has proven inadequate to explain the biological effects of Auger emitters.^{1,2,12,13} Since HILED clearly plays a major role, the cornerstone of any microdosimetry technique for Auger-emitters is the spectrum of low-energy electrons emitted in their decay including those which deposit their energy over just a few tens of nanometers (e.g., very low-energy N- and O-shell Auger electrons). The purpose of this report is to provide extremely detailed Auger electron spectra for commonly used radionuclides and to indicate the spatial dimensions over which these spectra can provide energy deposition information that cannot be obtained with conventional spectra given by MIRD¹⁴ and ICRP.¹⁵ The discussion of dosimetric techniques which utilize these spectra will be left to a later report of this Task Group.^{4,6,9,16-25}

B. Auger processes

When radionuclides decay by EC or IC, a vacancy is created in the inner atomic shell of the residual atom. Subsequently, the excited atom undergoes a series of transi-

tions until the ground state of the atom is reached.' These transitions fall under two categories: radiative and nonradiative processes. Radiative transitions, which predominate for K-shell vacancies, result in the emission of a characteristic x ray (Fig. 1). There are a variety of nonradiative transitions, the most common being of the Auger, Coster-Kronig (CK), and super Coster-Kronig (super CK) types (Fig. 1), each resulting in the ejection of an orbital electron. These processes are highly probable when the vacancy lies beyond the L-shell. In an Auger transition, an initial vacancy in a lower major shell is filled by an electron from a higher major shell and another electron is ejected from a higher major shell. While CK transitions are similar, the electron that fills the vacancy originates from the same major shell, and the ejected electron is from a higher major shell. Finally, in the super CK case, the vacancy and the two electrons are all in the same major shell. Radiative transitions move the vacancy to a higher major shell with no change in the number of vacancies while the nonradiative ones increase the number of vacancies by one. Hence, as the innermost vacancy percolates toward the valence shell, a cascade phenomenon develops with corresponding vacancy multiplication and emission of numerous low-energy electrons, collectively referred to as Auger electrons. Generally, several Auger electrons are emitted for each primary inner shell vacancy. Most of these have very low energies (less than a few hundred eV), intermediate values of linear energy transfer (10-25 keV/ μm), and extremely short ranges (several nm) in biological matter. Given that the cascade is completed within $\sim 10^{-15}$ s, the region in the immediate vicinity of the atom is showered with Auger electrons and, as a consequence, very high local energy densities are realized.^{3,4,7,9,26}

C. Auger electron spectra

In view of the importance of Auger electrons in causing biological damage, a number of early efforts were made

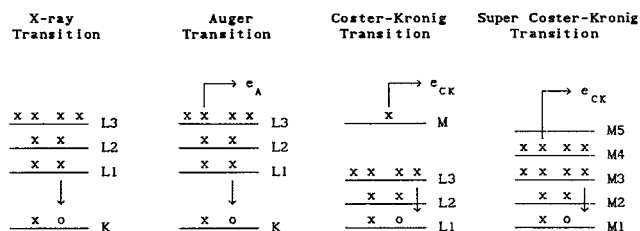


FIG. 1. Radiative and nonradiative transitions in atomic inner shell processes. There are no CK transitions in the K shell.

to calculate Auger electron spectra for radionuclides decaying by EC and IC.²⁷⁻²⁹ More recently, the MIRD Committee¹⁴ and ICRP¹⁵ have independently published volumes of radiation spectra for radionuclides and have included Auger electron yields and energies. Although the theoretical Auger electron spectra presented therein provide some guidance in regard to the dosimetry of Auger emitters, they did not address the N- and O-shell Auger electrons which have a significant contribution to HILED in the immediate vicinity of the decay site. Realizing this inadequacy, as well as the potential importance of stochastic differences in individual Auger cascades, Charlton and Booz³⁰ developed a Monte Carlo computer program to simulate the decay of the prolific Auger emitter ¹²⁵I in both the gaseous and condensed state. The Monte Carlo technique allows examination of the stochastic nature of individual decays and facilitates determination of an average Auger electron spectrum including the very low-energy Auger electrons. Spectra of similar detail, obtained using phenomenological methods, have been published for ⁷⁷Br (Ref. 31), ⁷⁵Se (Ref. 32), ⁵¹Cr (Ref. 19), ²⁰¹Tl (Refs. 33 and 34), ¹²⁵I (Ref. 35), ¹²³I (Ref. 36), ⁵⁵Fe (Ref. 37), and ⁴⁰K (Ref. 38). In a thorough review of biophysical aspects and dosimetry of Auger emitters, Sastry and Rao¹ presented a compilation of Auger spectra for a number of radionuclides. Following the lead of Charlton and Booz,³⁰ Humm^{39,40} used Monte Carlo techniques to calculate Auger spectra for the radionuclides ¹²⁵I, ¹²³I, ⁷⁷Br, and ⁶⁴Cu. Similar Monte Carlo techniques were also used by Howell *et al.*⁴¹ and Rao *et al.*⁴² for ^{193m}Pt and ^{195m}Pt, and ¹¹¹In, respectively. In a recent publication, Pomplun *et al.*⁵ revised the original ¹²⁵I calculations of Charlton and Booz.³⁰ They pointed out that although the original average radiation spectrum was very good, energy conservation was significantly violated for some individual ¹²⁵I decays in the original Monte Carlo calculation.³⁰ To rectify this problem, a computer program⁴³ was used to compute the energy of the atomic configuration at each stage of the simulated decay process. The Auger electron energy was assigned based on the energy difference of the atomic states before and after the transition. Using this recipe, and a great deal of supercomputer CPU time, Pomplun *et al.*⁵ were able to achieve energy balance for each simulated ¹²⁵I decay.

Although the above calculations provide a substantial database of detailed Auger electron spectra, there is some variation in the assumptions used by the various authors in

their calculations and therefore some discrepancies exist in the spectra and local energy depositions. Hence, there is a need to establish a generally agreed upon set of basic assumptions which may be used to create a self-consistent database of Auger electron spectra for all radionuclides of interest to medicine, biology, and the environment. The most recent technique of Pomplun *et al.*⁵ is one candidate for use in creating such a database. The feasibility of this approach for large scale calculations, however, is minimal due to the excessive supercomputer time required. Furthermore, there is no concrete evidence that these calculations provide a substantial improvement in overall accuracy due to the fact that the atomic processes in a single ¹²⁵I atom may be quite different than those for ¹²⁵I atoms embedded within molecular structures of biological systems. In view of these limitations and uncertainties, a combination of the assumptions and techniques used by Charlton and Booz,³⁰ Sastry and Rao,¹ Humm,^{39,40} and Howell *et al.*⁴¹ are used in the present report to calculate complete average Auger electron spectra for a variety of radionuclides of medical and environmental significance.

II. COMPUTATIONAL METHODS

A. Overview

Since the electronic deexcitation of an atom with an inner shell vacancy is governed by the combinatorial probabilities of electron and x-ray transitions to the lowest energy state of the atom, the Auger electron spectra are highly stochastic in nature. The Monte Carlo method is the only means to calculate the stochastic variation in Auger electron emission from atom to atom. Such data may be useful in the theoretical estimation of damage suffered by critical biological targets which may be comprised of entities within the subcellular realm. In the experimental realm, the response of mammalian cells to incorporated radionuclides is derived from a large population of cells where the exact number of decays which occur in any given cell is not known. Hence, the average response of the population is measured as a function of the average number of decays in the cell or organ. Therefore, for the purposes of obtaining dose-response relationships for mammalian cells, the absorbed dose is most aptly derived from average radiation spectra. In view of these considerations, the Auger spectra generated in this report are obtained by Monte Carlo methods, thereby yielding both stochastic information and average radiation spectra. The Monte Carlo method simulates the nuclear processes associated with the radioactive decay of the parent and the atomic and nuclear transitions which occur in the residual daughter atom. The simulation process is carried out with a Monte Carlo computer code⁴¹ similar to that of the work of Charlton and Booz.³⁰ Given the complexity of the code, it is perhaps most instructive to describe the technique by example. The Auger emitter ¹²⁵I serves as a good example since its decay involves both EC and IC processes and a great deal of data exists for this copious emitter of Auger electrons.

The radionuclide ¹²⁵I decays, with a 60-d physical half-life, to the ground state of ¹²⁵Te via a sequence of two

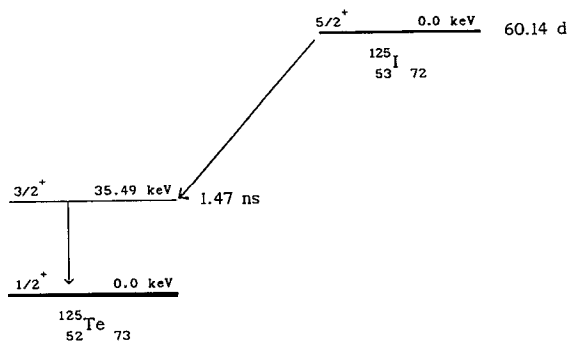


FIG. 2. Nuclear decay scheme for ^{125}I (Ref. 44).

nuclear processes (Fig. 2).⁴⁴ In the first step, ^{125}I decays via electron capture to the $3/2^+$ excited state of ^{125}Te which has a half-life of 1.47 ns (Fig. 2). This is followed by a transition to the ground state of ^{125}Te via either internal conversion or γ -emission with the probability of the latter being only about 6.66%.⁴⁴ As a result of each EC and IC event, a vacancy is created in an inner atomic orbital of the ^{125}Te atom. The resulting ionized atom is energetically unstable and therefore leads to a complex series of radiative and nonradiative transitions.

B. Monte Carlo simulation

The Monte Carlo calculation simulates the decay of ^{125}I using random selection processes. In general, at any stage of the decay, the simulated decay process proceeds by randomly selecting a transition from the set of all possible transitions for the nuclear and atomic configuration at that stage. As each random selection is made, data concerning the specific nuclear or atomic event, as well as the emitted radiations, are recorded.

Simulation of $^{125}_{53}\text{I}$ begins by initializing the atomic configuration of ^{125}I with its full complement of 53 electrons. Since ^{125}I can only decay to a single nuclear state of ^{125}Te , the EC process is straightforward and is carried out by removing a single electron from one of the atomic subshells. The decision as to which subshell the electron is captured from is based on relative capture probabilities ϵ_i for the i different subshells. Therefore, the sum of the relative probabilities is normalized to unity, a random number between 0 and 1 is generated, and the subshell selected based on the random number. If, for example, the capture ratios $\epsilon_K: \epsilon_{L_1}: \epsilon_{L_2}: \epsilon_{M_1}: \epsilon_{N_1}$ are 84:10:3:2:1, then the probabilities $p_K = 0.84$, $p_{L_1} = 0.10$, $p_{L_2} = 0.03$, $p_{M_1} = 0.02$, and $p_{N_1} = 0.01$, are obtained. If the random number falls between 0.0 and 0.84, a K-shell vacancy is created, while random numbers between 0.84 and 0.94, 0.94 and 0.97, 0.97 and 0.99, 0.99 and 1.0, result in creation of an L_1 -, L_2 -, M_1 -, N_1 -shell vacancy, respectively. Upon selection of the subshell in the manner described, the chosen EC transition is recorded, an electron is removed from the atomic subshell, and the "nuclear pointer" (denotes nuclear state) is moved to the excited state of ^{125}Te . The "atomic pointer" (denotes

vacancy location) is moved to the subshell containing the vacancy.

With a vacancy created in the ^{125}Te daughter atom, the Monte Carlo code now turns toward simulation of the atomic deexcitation processes. As indicated earlier, atomic deexcitation occurs via two competitive processes: (1) radiative x-ray transitions, and (2) nonradiative transitions. The probability of filling a vacancy in subshell i via an x-ray transition is given by its fluorescence yield ω_i , where $0 \leq \omega_i \leq 1$. Hence, a new random number is generated which, if less than ω_i , stipulates an x-ray transition. Otherwise a nonradiative transition is selected. For the sake of discussion, assume that the vacancy resides in the K-shell and an x-ray transition is chosen (x-ray transitions dominate for the K-shell). The relative probabilities for the various K-shell radiative transitions are constructed by normalizing the sum of the theoretical radiative rates to 1. As in the case of EC, a new random number is generated and the transition is selected accordingly. Bookkeeping is carefully maintained throughout with the transition information recorded, the initial vacancy filled, and a new vacancy created in the higher subshell than the one from which the electron which filled the vacancy originated. The "atomic pointer" is set to this higher subshell.

Since a new vacancy is created as a consequence of the radiative transition, the atomic deexcitation process continues. As in the case of the initial vacancy created by the EC event, a radiative or nonradiative transition is possible. To continue our description of the Monte Carlo simulation, assume that this time a nonradiative transition is selected. In that event, the sum of the nonradiative transition rates corresponding to all possible ways of filling the vacancy (Auger, CK, super CK) is normalized to unity, a random number is generated, and the transition is selected as described earlier. As shown in Fig. 1, although the primary vacancy is filled, a nonradiative transition results in the emission of an Auger electron and thereby creation of two new vacancies in higher subshells. With nonradiative transitions dominating above the L-shell, multiple vacancies are the norm, thus invalidating the theoretical transition rates which assume frozen orbitals.⁴⁵⁻⁴⁷ To compensate for this, correction factors based on the number of vacancies are applied to each transition rate prior to the normalization process (see Sec. II D 1).

It is important to note that the "atomic pointer" is always set to the innermost shell which contains a vacancy. Hence, the innermost vacancy steadily moves toward the valence or near-valence subshells during this cascade process. This process continues, with the transition information being recorded at each step, until no more electrons are available for transitions. The time scale for the complete atomic deexcitation process is $\sim 10^{-15}$ s while the half-life of the intermediate $3/2^+$ nuclear state of ^{125}Te is 1.47×10^{-9} s. The lifetime of the intermediate state is assumed to be long enough such that all the subshells are refilled with their requisite number of electrons, the electrons being supplied from the continuum. This completes the first phase in simulating the decay of ^{125}I .

The second phase of the ^{125}I decay simulation begins at

the $3/2^+$ excited state of ^{125}Te which in turn decays to the ground state of ^{125}Te by way of either IC or γ -emission. If IC were selected, an orbital electron is ejected from an inner atomic shell, whereas in the case of γ -emission a γ -ray is emitted. The relative probability for these two competitive nuclear processes is obtained from the experimental total internal conversion coefficient a . Yet another random number is generated and if this number is less than $1/(1 + \alpha)$, a γ -emission is chosen, otherwise IC is selected. In the case of ^{125}I , the probability of an IC transition is 94.34%.⁴⁴ If an IC transition is selected, the “nuclear pointer” is set to the ground state of ^{125}Te and the sum of the theoretical subshell IC coefficients α_i are normalized to 1 to obtain the relative probabilities p_i for ejection of an orbital electron from the i -shell. A random number is generated and the subshell is chosen in the same manner described earlier. The transition information is stored and the “atomic pointer” is set to the subshell in which the vacancy is created. The cascade of atomic transitions that follow are handled in the same manner as when the initial vacancy was created by the EC process. This completes the simulation of a single ^{125}I disintegration. It should be pointed out that marked stochastic differences may be observed in the emitted radiations from one disintegration to the next, therefore, 10 000 such disintegrations are considered when constructing the average radiation spectrum for the radionuclide.

The radionuclide ^{125}I was selected as an example because of its relative simplicity. More complicated decay schemes such as those of ^{67}Ga or ^{201}Tl may involve multiple pathways for both the EC transitions as well as the nuclear transitions in the daughter atom. In all cases, the relative strengths of these transitions are incorporated into the decision making process of the simulation.

C. Input data

1. Decay schemes and nuclear data

For each radionuclide, all decay schemes and nuclear data, including transition energies, multipole character of transitions, multipole mixing parameters δ , total disintegration energy Q^+ in EC decay, and branching ratios are obtained from Nuclear Data Sheets. The reference numbers corresponding to the Nuclear Data Sheets for ^{55}Fe , ^{67}Ga , $^{99\text{m}}\text{Tc}$, ^{111}In , $^{113\text{m}}\text{In}$, $^{115\text{m}}\text{In}$, ^{123}I , ^{125}I , $^{193\text{m}}\text{Pt}$, $^{195\text{m}}\text{Pt}$, ^{201}Tl , and ^{203}Pb are 48, 49, 59, 50, 60, 61, 51, 44, 62, 63, 52, and 53, respectively.

2. Electron capture ratios

Experimental subshell capture probabilities ϵ_K , ϵ_{L_1} , and ϵ_{M_1} are obtained from Nuclear Data Sheets.^{44,48-53} Where necessary, the ratio $\epsilon_{L_1}/\epsilon_{L_2}$ is calculated using the expressions of Martin and Blichert-Toft;⁵⁴ L_3 capture is ignored.⁵⁴ M-shell and N-shell capture are much less probable than K- and L-shell capture, and M_1 and N_1 capture dominate in M- and N-shell capture, respectively.⁵⁴ Therefore, it is assumed that $\epsilon_{M_1} = \epsilon_{M_1} + \epsilon_{N_1}$. Since M-shell capture is much more probable than N-shell, it is further assumed that $\epsilon_{N_1} = 0.1 \epsilon_{M_1}$.

3. Internal conversion coefficients

Experimental total internal conversion coefficients a , obtained for each radionuclide from the Nuclear Data Sheets listed above, are utilized for all nuclear transitions involving IC processes. In the case of subshell coefficients α_j , the theoretical values of Rösler *et al.*⁵⁵ are employed. Whenever transitions are of mixed multipoles, corrections for such admixtures are made according to the relation

$$\alpha_{jk} = (\alpha_j + \delta^2 \alpha_k) / (1 + \delta^2), \quad (1)$$

where j and k denote the multipole characters (e.g., M1 and E2).

4. Auger, CK, and super-CK transition rates

Theoretical radiationless transition rates of Chen *et al.*⁴⁵ were used for the K- and L-shell, while the rates of McGuire^{46,47} were employed for the M- and N-shells. No such transition rates are available for the O-shell. Hence, using the approximation of Kassir *et al.*,³⁴ the O-shell transition probabilities are estimated based on the number and distribution of electrons available for the transition. No quantum mechanical considerations are made in this first approximation. The small probability of double-Auger electron and shake-off electron emissions are ignored.

5. X-ray transition rates

Scofield⁵⁶ gives the theoretical x-ray transition rates for the K- and L-shells. Those for M-shell x-rays are calculated by Manson and Kennedy⁵⁷ for electric dipole transitions. In the N-shell and above, Auger and CK processes dominate while x-ray transitions are negligible.

6. Fluorescence yields

Fluorescence yield data for all radionuclides are obtained from Bambynek *et al.*⁵⁸ Experimental K-shell fluorescence yields, given only for selected values of Z , are used whenever possible. Otherwise, values from a fit to the experimental data are used.⁵⁸ The yields for the L- and M-shell are interpolated from the theoretical values tabulated in Ref. 58.

7. Energies of emitted radiations

The γ -ray energies are taken from Nuclear Data Sheets.^{44,49-53,59-63} Conversion electron energies $E_a^Z(\text{IC})$ are calculated according to $E_a^Z(\text{IC}) = \Delta E - B_a^Z$, where Z is the atomic number, “ a ” specifies the subshell from which the electron is ejected, ΔE is the energy difference between the two nuclear states, and B_a^Z is the electron binding energy for subshell “ a .” The binding energies of Sevier⁶⁴ are used in all cases. X-ray energies $E_{ab}^Z(\text{XR})$ are given by $E_{ab}^Z(\text{XR}) = B_a^Z - B_b^Z$, where “ a ” and “ b ” specify the transition. Finally, Auger electron energies are estimated with the $Z/Z + 1$ rule:^{1,30,41,65}

$$E_{abc}^Z = B_a^Z - \frac{1}{2}(B_b^Z + B_b^{Z+1} + B_c^Z + B_c^{Z+1}). \quad (2)$$

where “ a ,” “ b ,” and “ c ” specify the transition.

M3	x x x o			
M2	x o	KL _{1,2} (A)	1	
M1	x x	KL _{2,3} (A)	1/4	
L3	x o o o	KL ₃ (A)	0	
L2	x x	KL ₃ M ₂ (A)	1/2 * 1/4	
L1	x x	KM ₃ M ₃ (A)	(3! / 2!(3-2)!) / (4! / 2!(4-2)!)	
K	x o	KL ₃ (X)	1/4	

FIG. 3. Transition rate correction factors (right) for a hypothetical atomic vacancy distribution (left). The presence of an electron is denoted by an x while a vacancy is indicated by an o. The letters X and A in the parenthesis indicate a radiative and nonradiative transition, respectively.

D. Estimates and assumptions

1. Frozen atomic orbitals

As a consequence of the vacancy cascade process described above, multiple vacancies may exist within the atomic shells. The theoretical atomic transition rates^{45-47,56,57} used in this report assume frozen orbitals. Therefore, the relative transition rates may be somewhat different than the published values. Hence, an empirical correction, first used by Krause and Carlson⁶⁶ and subsequently in all of the Monte Carlo calculations of Auger spectra,^{5,30,39,41,42} is made for each transition based on the fraction of electrons remaining in the orbitals involved. Examples of corrections for several transitions are shown in Fig. 3 for a hypothetical atomic vacancy distribution.

2. Auger electron energies

In principle, each Auger electron energy should be calculated based on the electron configuration for that particular event. The extensive CPU time required precludes this approach. Therefore, in keeping with the spectral calculations of others,^{1,30,39} Auger and CK electron energies are computed using the well established $Z/Z + 1$ rule. Under certain circumstances transitions for which there are published transition rates yield negative electron energies when calculated in this manner. For instance, in the case of the radioplatinums ($Z = 78$), excluded transitions include $L_1L_2N_3$, $M_1M_3M_2$, $M_2M_3M_4$, $M_1M_5O_3$, and $N_2N_3N_{6,7}$. These transitions comprise about 4%, 4%, 1%, 1%, and 4%, respectively, of the total radiationless transition rate for the subshell in question. Exclusion of these transitions does not have a major effect on the spectrum as a whole.

3. Charge neutralization

During the Auger cascade process a large number of electrons are ejected from the atomic orbitals, thereby resulting in multiply ionized states. Carlson and White⁶⁷ have experimentally demonstrated this phenomena for the gaseous state of Hg ($Z = 80$). They found that the average charge on the Hg atom following creation of L, M, and N, initial vacancies is 9.8^+ , 7.3^+ , and 4.7^+ , respectively. For L vacancies, charge states as high as 17^+ were observed with a very small probability. Although experiments in the condensed phase were not performed, the authors discussed the extent of multiple ionization in this phase. They

TABLE I. Fe-55 average radiation spectrum.

	Average energy (MeV)	Yield/decay	Range (microns)
Auger KLL	5.13E-03	4.87E-01	8.74E-01
Auger KLX	5.77E-03	1.20E-01	1.06E+00
Auger KXY	6.42E-03	8.20E-03	1.27E+00
CK LLX	5.52E-05	3.10E-01	3.61E-03
Auger LMM	5.61E-04	1.41E+00	2.91E-02
Auger LMX	6.06E-04	1.94E-02	3.41E-02
CK MMX	4.18E-05	2.54E+00	2.74E-03
Auger MXY	4.89E-05	2.33E-01	3.25E-03
X-ray K _{α1}	5.90E-03	1.57E-01	
X-ray K _{α2}	5.89E-03	8.74E-02	
X-ray K _{β1}	6.49E-03	1.92E-02	
X-ray K _{β3}	6.49E-03	1.05E-02	
X-ray L	6.35E-04	3.30E-03	

Total yield of Auger and CK electrons per decay= 5.1

Total yield of x-rays per decay=0.28

Total energy released per decay=5810 eV

Auger and CK energy released per decay=4177 eV

X-ray energy released per decay= 1633 eV

TABLE II. Ga-67 average radiation spectrum.

	Average energy (MeV)	Yield/decay	Range (microns)
γ_1	9.33E-02	3.63E-01	
γ_2	9.13E-02	3.19E-02	
γ_3	1.85E-01	2.27E-01	
γ_4	2.09E-01	2.36E-02	
γ_5	3.00E-01	1.82E-01	
γ^p	3.94E-01	5.42E-02	
γ_7	4.94E-01	1.10E-03	
γ_{10}	8.886-01	1.910E-03	
IC 1 K	8.37E-02	2.70E-01	1.05E+02
IC 1 L	9.22E-02	3.76E-02	1.24E+02
IC 1 M,N...	9.32E-02	6.60E-03	1.27E+02
IC 2 K	8.16E-02	2.70E-03	1.01E+02
IC 3 K	1.75E-01	3.40E-03	3.63E+02
IC 5 K	2.91E-01	1.00E-03	8.14E+02
Auger KLL	7.43E-03	4.70E-01	1.63E+00
Auger KLX	8.44E-03	1.16E-01	2.02E+00
Auger KXY	9.46E-03	8.20E-03	2.45E+00
CK LLX	7.29E-05	3.46E-01	4.31E-03
Auger LMM	9.21E-04	1.68E+00	6.06E-02
Auger LMX	9.53E-04	1.16E-02	6.36E-02
CK MMX	6.24E-05	2.07E+00	3.91E-03
X-ray K _{α1}	8.64E-03	3.35E-01	
X-ray K _{α2}	8.62E-03	1.67E-01	
X-ray K _{β1}	9.57E-03	4.00E-02	
X-ray K _{β3}	9.57E-03	2.28E-02	
X-ray L	1.00E-03	1.10E-02	

Total yield of Auger and CK electrons per decay=4.7

Total yield of IC electrons per decay=0.32

Total yield of x-rays per decay=0.57

Total yield of γ -rays per decay=0.88

Total energy released per decay=201624 eV

Auger and CK energy released per decay=6264 eV

IC energy released per decay=28078 eV

X-ray energy released per decay=4936 eV

y-ray energy released per decay= 162347 eV

TABLE III. Tc-99m average radiation spectrum.

	Average energy (MeV)	Yield/decay	Range (microns)
γ_2	1.41E-01	8.89E-01	
IC 1 M,N...	1.82E-03	9.91E-01	1.65E-01
IC 2 K	1.19E-01	8.43E-02	1.93E+02
IC 2 L	1.37E-01	1.36E-02	2.44E+02
IC 2 M,N...	1.40E-01	3.70E-03	2.51E+02
IC 3 K	1.22E-01	5.90E-03	1.998+02
IC 3 L	1.40E-01	2.50E-03	2.50E+02
Auger KLL	1.53E-02	1.26E-02	5.57E+00
Auger KLX	1.78E-02	4.70E-03	7.25E+00
CK LLX	4.29E-05	1.93E-02	2.83E-03
Auger LMM	2.05E-03	8.68E-02	1.99E-01
Auger LMX	2.32E-03	1.37E-02	2.41E-01
Auger LXY	2.66E-03	1.20E-03	3.00E-01
CK MMX	1.16E-04	7.47E-01	5.98E-03
Auger MXY	2.26E-04	1.10E+00	1.05E-02
CK NNX	3.34E-05	1.98E+00	2.05E-03
X-ray K _{α1}	1.84E-02	3.89E-02	
X-ray K _{α2}	1.83E-02	2.17E-02	
X-ray K _{β1}	2.06E-02	7.60E-03	
X-ray K _{β2}	2.10E-02	1.50E-03	
X-ray K _{β3}	2.06E-02	2.70E-03	
X-ray L	2.45E-03	4.90E-03	
X-ray M	2.36E-04	1.20E-03	

Total yield of Auger and CK electrons per decay=4.0

Total yield of IC electrons per decay=1.1

Total yield of x-rays per decay=0.079

Total yield of y-rays per decay=0.89

Total energy released per decay= 142646 eV

Auger and CK energy released per decay=899 eV

IC energy released per decay= 15383 eV

X-ray energy released per decay= 1367 eV

y-ray energy released per decay= 124997 eV

concluded that the initial phases of the cascade would be virtually the same as in the gas phase; however, when the vacancies reach the conduction band, vacancy filling is immediate. As a consequence, charge buildup on the atom during the cascade process is greatly reduced. Based on these findings, and the early work of Charlton and Booz,³⁰ the present calculations assume that any vacancies created in the valence shell are filled immediately (fast neutralization). This has been the approach taken in all of the recent calculations of Auger spectra for the condensed phase,^{5,30,39,41,42} with the exception of Pomplun *et al.*⁵ The decision as to the subshells to be filled in the fast neutralization process is made empirically. Typically the outermost subshells have binding energies ranging from zero to a few eV and are therefore selected to be filled immediately following the creation of a hole. For ¹²⁵I, the O-shell is the valence shell. Since O-shell Auger transitions have been included in this report, the atom is completely neutralized at the end of the cascade process. This approach eliminates the need to address the fate of the potential energy associated with residual charge on the atom.

The above approach for the condensed phase is slightly different than the original Monte Carlo calculation of Charlton and Booz³⁰ where O-shell transitions were not considered. In their calculations, some vacancies were left on the residual atom at the end of the cascade process.

TABLE IV. In-111 average radiation spectrum.

	Average energy (MeV)	Yield/decay	Range (microns)
γ_1	1.71E-01	9.06E-01	
γ_2	2.45E-01	9.37E-01	
IC 1 K	1.45E-01	8.24E-02	2.05E+02
IC 1 L	1.67E-01	1.00E-02	2.72E+02
IC 1 M,N...	1.71E-01	1.40E-03	2.83E+02
IC 2 K	2.19E-01	5.21E-02	5.20E+02
IC 2 L	2.41E-01	9.10E-03	6.09E+02
IC 2 M,N...	2.45E-01	1.90E-03	6.22E+02
Auger KLL	1.91E-02	1.03E-01	8.21E+00
Auger KLX	2.23E-02	3.94E-02	1.08E+01
Auger KXY	2.55E-02	3.60E-03	1.36E+01
CK LLX	1.83E-04	1.51E-01	8.69E-03
Auger LMM	2.59E-03	8.35E-01	2.87E-01
Auger LMX	3.06E-03	1.90E-01	3.75E-01
Auger LXY	3.53E-03	1.09E-02	4.73E-01
CK MMX	1.25E-04	9.15E-01	6.35E-03
Auger MXY	3.50E-04	2.09E+00	1.64E-02
CK NNX	3.88E-05	2.54E+00	2.50E-03
Auger NXY	8.47E-06	7.82E+00	2.51E-04
X-ray K _{α1}	2.32E-02	4.63E-01	
X-ray K _{α2}	2.30E-02	2.40E-01	
X-ray K _{β1}	2.61E-02	7.88E-02	
X-ray K _{β2}	2.66E-02	1.86E-02	
X-ray K _{β3}	2.61E-02	3.82E-02	
X-ray K _{β5}	2.63E-02	1.10E-03	
X-ray L	3.23E-03	4.99E-02	
X-my M	3.56E-04	3.00E-03	

Total yield of Auger and CK electrons per decay= 14.7

Total yield of IC electrons per decay=0.16

Total yield of x-rays per decay=0.89

Total yield of y-rays per decay= 1.84

Total energy released per decay=419205 eV

Auger and CK energy released per decay=6750 eV

IC energy released per decay=25957 eV

X-ray energy released per decay= 19966 eV

y-ray energy released per decay=366532 eV

Therefore, one must also address charge neutralization between successive nuclear events such as between the EC and IC processes of ¹²⁵I. In these instances the lifetime of the intermediate state is usually at least a few orders of magnitude longer than the time scale over which the cascade process occurs (~10⁻¹⁵ s). It is therefore reasonable to assume that the atom recovers its normal electronic configuration after each nuclear transition. Virtually all estimates of Auger spectra in the condensed phase have made this assumption, and this approximation has been used in the present report when necessary.

It should be noted that the charge neutralization scheme can have a significant impact on the number of Auger electrons emitted. Charlton and Booz³⁰ performed Monte Carlo calculations for both the condensed and gaseous phases of ¹²⁵I. In the gaseous state the atom was assumed to be isolated and therefore fast neutralization was not performed, nor were the vacancies filled between the EC and IC processes. Under these circumstances an average electron yield of 13.2 was obtained compared to 21.2 for the condensed phase, the difference in number due largely to differences in the N Auger and CK electron yields. Given that the intent of this report is to obtain spectra for

TABLE V. In-113m average radiation spectrum.

	Average energy (MeV)	Yield/decay	Range (microns)
γ_1	3.92E-01	6.45E-01	
IC 1 K	3.64E-01	2.85E-01	1.15E+03
IC 1 L	3.88E-01	5.39E-02	1.26E+03
IC 1 M,N...	3.91E-01	1.67E-02	1.28E+03
Auger KLL	1.98E-02	2.59E-02	8.76E+00
Auger KLX	2.32E-02	1.28E-02	1.15E+01
Auger KXY	2.68E-02	1.20E-03	1.48E+01
CK LLX	1.97E-04	4.48E-02	9.28E-03
Auger LMM	2.71E-03	2.44E-01	3.08E-01
Auger LMX	3.20E-03	5.99E-02	4.04E-01
Auger LX Y	3.70E-03	3.40E-03	5.11E-01
CK MMX	1.24E-04	2.73E-01	6.31E-03
Auger MXY	3.76E-04	6.22E-01	1.77E-02
CK NNX	3.58E-05	7.38E-01	2.25E-03
Auger NXY	1.63E-05	2.30E+00	6.97E-04
X-ray K _{α_1}	2.42E-02	1.33E-01	
X-ray K _{α_2}	2.40E-02	6.98E-02	
X-ray K _{β_1}	2.73E-02	2.46E-02	
X-ray K _{β_2}	2.79E-02	6.10E-03	
X-ray K _{β_3}	2.72E-02	1.13E-02	
X-ray L	3.35E-03	1.40E-02	
Total yield of Auger and CK electrons per decay=4.3			
Total yield of IC electrons per decay=0.36			
Total yield of x-rays per decay=0.26			
Total yield of y-rays per decay=0.64			
Total energy released per decay= 391645 eV			
Auger and CK energy released per decay=2047 eV			
IC energy released per decay= 130982 eV			
X-ray energy released per decay=6093 eV			
y-ray energy released per decay=252523 eV			

TABLE VI. In-115m average radiation spectrum.

	Average energy (MeV)	Yield/decay	Range (microns)
γ_1	3.36E-01	4.96E-01	
IC 1 K	3.08E-01	4.05E-01	8.92E+02
IC 1 L	3.32E-01	7.88E-02	9.996+02
IC 1 M,N...	3.36E-01	2.10E-02	1.01E+03
Auger KLL	1.99E-02	3.45E-02	8.79E+00
Auger KLX	2.33E-02	1.87E-02	1.16E+01
Auger KXY	2.65E-02	9.00E-04	1.44E+01
CK LLX	1.93E-04	6.09E-02	9.14E-03
Auger LMM	2.70E-03	3.46E-01	3.06E-01
Auger LMX	3.20E-03	8.26E-02	4.03E-01
Auger LX Y	3.72E-03	6.30E-03	5.15E-01
CK MMX	1.26E-04	3.89E-01	6.37E-03
Auger MXY	3.77E-04	8.79E-01	1.77E-02
CK NNX	3.55E-05	1.04E+00	2.23E-03
Auger NXY	1.62E-05	3.25E+00	6.90E-04
X-ray K _{α_1}	2.42E-02	1.96E-01	
X-ray K _{α_2}	2.40E-02	9.54E-02	
X-ray K _{β_1}	2.73E-02	3.29E-02	
X-ray K _{β_2}	2.79E-02	8.70E-03	
X-ray K _{β_3}	2.72E-02	1.68E-02	
X-ray L	3.40E-03	2.33E-02	
X-ray M	4.58E-04	1.20E-03	
Total yield of Auger and CK electrons per decay=6.1			
Total yield of IC electrons per decay=0.50			
Total yield of x-rays per decay=0.38			
Total yield of y-rays per decay=0.50			
Total energy released per decay=336176 eV			
Auger and CK energy released per decay=2847 eV			
IC energy released per decay= 157958 eV			
X-ray energy released per decay= 8730 eV			
y-ray energy released per decay= 166641 eV			

TABLE VII. I-123 average radiation spectrum.

	Average energy (MeV)	Yield/decay	Range (microns)
γ_1	1.59E-01	8.39E-01	
γ_3	4.40E-01	3.90E-03	
γ_4	3.46E-01	1.40E-03	
γ_5	5.05E-01	2.80E-03	
γ_8	5.29E-01	1.45E-02	
γ_{12}	5.39E-01	4.50E-03	
γ_{16}	7.84E-01	1.00E-03	
IC 1 K	1.27E-01	1.30E-01	2.14E+02
IC 1 L	1.54E-01	1.79E-02	2.94E+02
IC 1 M,N...	1.58E-01	5.30E-03	3.08E+02
Auger KLL	2.24E-02	8.38E-02	1.09E+01
Auger KLX	2.63E-02	3.84E-02	1.43E+01
Auger KXY	3.02E-02	3.50E-03	1.81E+01
CK LLX	2.13E-04	1.56E-01	9.99E-03
Auger LMM	3.04E-03	7.51E-01	3.72E-01
Auger LMX	3.66E-03	2.02E-01	5.02E-01
Auger LX Y	4.28E-03	1.30E-02	6.48E-01
CK MMX	1.27E-04	8.69E-01	6.42E-03
Auger MXY	4.61E-04	1.97E+00	2.25E-02
CK NNX	2.98E-05	2.10E+00	1.75E-03
Auger NXY	3.25E-05	6.54E+00	1.98E-03
CK OOX	6.00E-06	2.18E+00	1.50E-04
X-ray K _{α_1}	2.75E-02	4.62E-01	
X-ray K _{α_2}	2.72E-02	2.37E-01	
X-ray K _{β_1}	3.10E-02	8.13E-02	
X-ray K _{β_2}	3.17E-02	2.27E-02	
X-ray K _{β_3}	3.09E-02	4.45E-02	
X-ray KM,N,O	3.17E-02	1.30E-03	
X-ray L	3.93E-03	7.90E-02	
X-ray M	5.43E-04	2.30E-03	
Total yield of Auger and CK electrons per decay= 14.9			
Total yield of IC electrons per decay=0.15			
Total yield of x-rays per decay=0.93			
Total yield of y-rays per decay=0.87			
Total energy released per decay=200396 eV			
Auger and CK energy released per decay=7419 eV			
IC energy released per decay=20245 eV			
X-ray energy released per decay=24134 eV			
y-ray energy released per decay= 148598 eV			

the purpose of dosimetry, utilization of fast neutralization (i.e., condensed phase) is appropriate.

III. RESULTS

Complete summaries of the average theoretical radiation spectra for the Auger emitters ^{55}Fe , ^{67}Ga , $^{99\text{m}}\text{Tc}$, ^{111}In , $^{113\text{m}}\text{In}$, $^{115\text{m}}\text{In}$, ^{123}I , ^{125}I , $^{193\text{m}}\text{Pt}$, $^{195\text{m}}\text{Pt}$, ^{201}Tl , and ^{203}Pb , are given in Tables I-XII, respectively. Each summary contains the average energy and yield information for all radiations based on 10 000 disintegrations. Radiations with yields of less than 10^{-3} have been excluded because they constitute a negligible contribution to the absorbed dose compared to the more abundant radiations. There are several contributions to the uncertainties in the yields and energies of the listed radiations, the major contributions coming from the basic assumptions outlined in Sec. II D as well as the theoretical and empirical nuclear and atomic data used in these calculations. However, it is generally acknowledged that the biological uncertainties with respect

TABLE VIII. I-125 average radiation spectrum.

	Average energy (MeV)	Yield/decay	Range (microns)
γ_1	3.55E-02	6.41E-02	
IC 1 K	3.65E-03	1.91E-01	4.98E-01
IC 1 L	3.06E-02	1.10E-01	1.86E+01
IC 1 M,N...	3.41E-02	2.84E-02	2.31E+01
Auger KLL	2.24E-02	1.38E-01	1.08E+01
Auger KLX	2.64E-02	5.90E-02	1.43E+01
Auger KXY	3.02E-02	6.50E-03	1.82E+01
CK LLX	2.19E-04	2.64E-01	1.02E-02
Auger LMM	3.05E-03	1.25E+00	3.73E-01
Auger LMX	3.67E-03	3.40E-01	5.04E-01
Auger LXY	4.34E-03	2.11E-02	6.62E-01
CK MMX	1.27E-04	1.44E+00	6.43E-03
Auger MXY	4.61E-04	3.28E+00	2.25E-02
CK NNX	2.99E-05	3.51E+00	1.15E-03
Auger NXY	3.24E-05	1.09E+01	1.97E-03
CK OOX	6.00E-06	3.66E+00	1.50E-04
X-ray K _{α1}	2.75E-02	7.51E-01	
X-ray K _{α2}	2.72E-02	3.94E-01	
X-ray K _{β1}	3.10E-02	1.38E-01	
X-ray K _{β2}	3.17E-02	4.03E-02	
X-ray K _{β3}	3.09E-02	6.85E-02	
X-ray K _{β5}	3.12E-02	1.20E-03	
X-ray KM,N,O	3.17E-02	3.00E-03	
X-ray L	3.93E-03	1.32E-01	
X-ray M	5.42E-04	4.00E-03	

Total yield of Auger and CK electrons per decay=24.9
 Total yield of IC electrons per decay=0.94
 Total yield of x-rays per decay= 1.53
 Total yield of γ -rays per decay=0.065
 Total energy released per decay=61439 eV
 Auger and CK energy released per decay= 12241 eV
 IC energy released per decay=7242 eV
 X-ray energy released per decay=39661 eV
 γ -ray energy released per decay= 2294 eV

to clearance, distribution, etc., far outweigh any errors in the radiation spectra in the final estimation of the absorbed dose from incorporated radionuclides. Finally, the range of the electrons in unit density matter is determined from the experimental range-energy relation of Cole.⁶⁸ An explanation of the notation used in these tables follows:

γ_a	Gamma-ray emission where the letter "a" denotes the nuclear transition number.
IC-b K, IC-b L, IC-b M,N...	Internal conversion transition where the letter "b" denotes the nuclear transition number. The notations K, L, and M,N... indicate that the electron was ejected from the K-shell, L-shell, or any other shell, respectively.
Auger KLL	K-shell Auger transition where the two new vacancies are in the L-shell.
Auger KLX	K-shell Auger transition where one of the two new vacancies is in the L-shell.
Auger KXY	K-shell Auger transition where neither of the two new vacancies is in the L-shell.

TABLE IX. Pt-193m average radiation spectrum.

	Average energy (MeV)	Yield/decay	Range (microns)
γ_1	1.35E-01	1.10E-03	
IC 1 K	5.71E-02	1.49E-01	5.47E+01
IC 1 L	1.23E-01	6.19E-01	2.03E+02
IC 1 M,N...	1.33E-01	2.32E-01	2.31E+02
IC 2 M,N...	1.00E-02	1.00E+00	2.72E+00
IC 3 M,N...	1.04E-03	1.00E+00	7.20E-02
Auger KLL	5.18E-02	2.70E-03	4.63E+01
Auger KLX	6.26E-02	1.80E-03	6.41E+01
CK LLX	1.41E-03	1.14E-01	1.12E-01
Auger LMM	7.13E-03	3.52E-01	1.52E+00
Auger LMX	9.20E-03	1.41E-01	2.34E+00
Auger LXY	1.12E-02	1.04E-02	3.29E+00
CK MMX	4.15E-04	1.68E+00	1.99E-02
Auger MXY	1.75E-03	1.96E+00	1.56E-01
CK NNX	1.71E-04	5.95E+00	8.21E-03
Auger NXY	5.65E-05	1.02E+01	3.67E-03
CK OOX	4.94E-05	6.07E+00	3.29E-03
X-ray K _{α1}	6.68E-02	6.89E-02	
X-ray K _{α2}	6.51E-02	4.45E-02	
X-ray K _{β1}	1.57E-02	1.61E-02	
X-ray K _{β2}	7.19E-02	5.80E-03	
X-ray K _{β3}	7.54E-02	7.60E-03	
X-ray L	1.01E-02	2.37E-01	
X-ray M	2.07E-03	4.47E-02	

Total yield of Auger and CK electrons per decay=26.4
 Total yield of IC electrons per decay= 3.0
 Total yield of x-rays per decay=0.43
 Total energy released per decay= 149436 eV
 Auger and CK energy released per decay= 10353 eV
 IC energy released per decay= 126738 eV
 X-ray energy released per decay= 12345 eV

CK LLX	All L-shell CK and super-CK transitions.
Auger LMM	L-shell Auger transitions where both of the two new vacancies are in the M-shell.
Auger LMX	L-shell Auger transition where one of the two new vacancies is in the M-shell.
Auger LXY	L-shell Auger transition where neither of the two new vacancies are in the M-shell.
CK MMX	All M-shell CK and super-CK transitions.
Auger MXY	All M-shell Auger transitions.
CK NNX	All N-shell CK and super-CK transitions.
Auger NXY	All N-shell Auger transitions.
CK OOX	All O-shell CK and super-CK transitions.
Auger OXY	All O-shell Auger transitions.
X-ray K _{αc}	K _α x-ray transition. The letter "c" indicates the type of transition (i.e., c = 1 for K _{α1}).
X-ray K _{βc}	K _β x-ray transition. The letter "c" indicates the type of transition (i.e., c = 1 for K _{β1}).
X-ray KM,N,O	All other K X-rays.
X-ray L	L x-rays.
X-ray M	M x-rays.

TABLE X. Pt-195m average radiation spectrum.

	Average energy (MeV)	Yield/decay	Range (microns)
γ_1	1.30E-01	2.51E-02	
γ_3	9.89E-02	1.17E-01	
γ_4	3.09E-02	2.45E-02	
IC 1 K	5.11E-02	1.26E-01	4.52E+01
IC 1 L	1.17E-01	6.20E-01	1.87E+02
IC 1 M,N...	1.27E-01	2.54E-01	2.14E+02
IC 2 K	5.14E-02	1.03E-02	4.56E+01
IC 2 L	1.17E-01	2.01E-02	1.86E+02
IC 2 M,N...	1.27E-01	7.80E-03	2.15E+02
IC 3 K	2.05E-02	6.65E-01	9.29E+00
IC 3 L	8.52E-02	1.16E-01	1.09E+02
IC 3 M,N...	9.62E-02	3.14E-02	1.34E+02
IC 4 L	1.71E-02	6.96E-01	6.79E+00
IC 4 M,N...	2.82E-02	2.15E-01	1.62E+01
Auger KLL	5.21E-02	1.57E-02	4.67E+01
Auger KLLX	6.28E-02	7.80E-03	6.44E+01
Auger KXY	7.33E-02	1.20E-03	8.41E+01
CK LLX	1.41E-03	5.51E-01	1.13E-01
Auger LMM	1.36E-03	9.89E-01	1.60E+00
Auger LMX	9.50E-03	4.15E-01	2.47E+00
Auger LXY	1.15E-02	3.58E-02	3.43E+00
CK MMX	4.07E-04	1.80E+00	1.94E-02
Auger MXY	1.73E-03	3.40E+00	1.54E-01
CK NNX	1.72E-04	6.05E+00	8.23E-03
Auger NXY	5.67E-05	1.29E+01	3.68E-03
CK OOX	4.94E-05	6.58E+00	3.29E-03
X-ray K _{α1}	6.68E-02	3.84E-01	
X-ray K _{α2}	6.51E-02	2.27E-01	
X-ray K _{β1}	7.51E-02	8.36E-02	
X-ray K _{β2}	7.18E-02	2.88E-02	
X-ray K _{β3}	1.54E-02	4.51E-02	
X-ray K _{β5}	7.62E-02	2.10E-03	
X-ray KM,N,O	7.70E-02	4.90E-03	
X-ray L	1.04E-02	6.65E-01	
X-ray M	2.06E-03	1.56E-02	

Total yield of Auger and CK electrons per decay= 32.8
Total yield of IC electrons per decay=2.8
Total yield of x-rays per decay= 1.5
Total yield of y-rays per decay=0.17
Total energy released per decay=258738 eV
Auger and CK energy released per decay=22526 eV
IC energy released per decay= 160427 eV
X-ray energy released per decay=601 12 eV
y-ray energy released per decay= 15674 eV

IV. DISCUSSION

The average radiation spectra presented in Tables I-XII are theoretical in nature. The yields and energies of the major radiations are in reasonably good agreement with the values established by the MIRD Committee¹⁴ and ICRP.¹⁵ Significant deviations are found primarily in the N- and O-shell Auger and CK electron yields which are absent in the MIRD¹⁴ and ICRP¹⁵ spectra. These very low-energy electrons play a critical role in the microscopic dosimetry of Auger emitters, and therefore their yields and energies are essential. To the best of our knowledge there are no experimental data available in the condensed phase with which to compare our calculations. However, the assumptions made in these calculations are reasonable and our result for ¹²⁵I of 21.2 Auger and CK electrons (exclud-

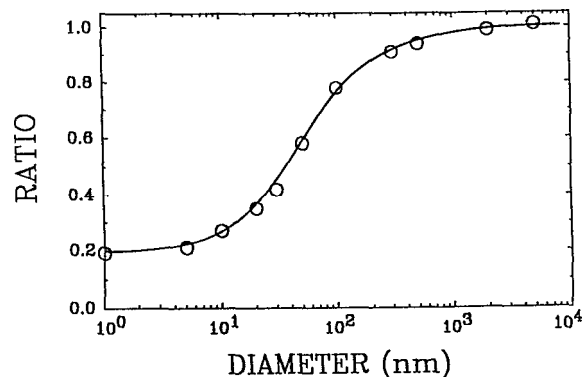


FIG. 4. Influence of Auger electron spectrum on the calculated average absorbed dose to spherical regions of unit density matter containing uniformly distributed ¹²⁵I. The abscissa is the sphere diameter. The ordinate is the ratio of dose calculated with the MIRD¹⁴ ¹²⁵I radiation spectrum to the dose calculated with the spectrum presented in Table VIII of this report. Note that the calculated dose is independent of the spectrum employed for sphere diameters greater than 1 μm , however, the very low-energy Auger electrons included in Table VIII play an increasingly important role as the volume is reduced.

ing the CK OOX electrons) is in good agreement with the calculations of Charlton and Booz³⁰ and Sastry and Rao.¹ Since the primary utility of these spectra is for dosimetry, more meaningful comparisons can be made by calculating the dose to small volumes containing radioactivity rather than comparing the number of electrons emitted.

A. Small volume dosimetry for different ¹²⁵I spectra

Unlike many of the radionuclides in Tables I-XII, a number of different spectra have been reported for ¹²⁵I. Therefore, ¹²⁵I is a convenient radionuclide to examine the effect of different spectra on the dose delivered to very small volumes of unit density matter. The computer program of Howell *et al.*,⁶⁹ designed to accommodate very low-energy electrons, is employed to calculate average absorbed doses to 10- and 20-nm diameter spheres of unit density matter containing uniformly distributed ¹²⁵I. Four different average spectra are compared (Table XIII): Sastry and Rao,¹ Pomplun *et al.*,⁵ MIRD,¹⁴ and the ¹²⁵I spectrum in this report (Table VIII). The absorbed doses obtained with the spectra of Sastry and Rao¹ and the present work are in good agreement, differing by less than 2%. No comparison could be made with the calculations of Charlton and Booz³⁰ or Humm³⁹ since average spectra were not provided. However, since their spectra are calculated in a similar manner, and the total electron yields were essentially the same, no significant differences are expected. The spectra of Pomplun *et al.*⁵ results in 1.7 and 2.0 times higher dose to 10-nm and 20-nm diameter spheres, respectively. This large difference is attributed entirely to the 1.1 keV of potential energy associated with multiple ionization of the residual tellurium atom assumed to be deposited locally within the sphere. As the volume of interest increases the difference diminishes. Hence, since the volume in which the potential energy is actually deposited is not known, the significance of the difference is unclear. Finally, a comparison may be made with the doses calculated using

TABLE XI. Tl-201 average radiation spectrum.

	Average energy (MeV)	Yield/decay	Range (microns)
γ_3	3.06E-02	2.70E-03	
γ_4	3.22E-02	2.40E-03	
γ_5	1.35E-01	2.72E-02	
γ_6	1.66E-01	1.30E-03	
γ_7	1.67E-01	9.56E-02	
IC 1 M,N...	8.95E-04	6.08E-01	5.82E-02
IC 2 L	1.22E-02	2.20E-03	3.77E+00
IC 3 L	1.59E-02	8.61E-02	5.96E+00
IC 3 M,N...	2.77E-02	2.36E-02	1.57E+01
IC 4 L	1.74E-02	7.24E-02	7.02E+00
IC 4 M,N...	2.94E-02	2.37E-02	1.74E+01
IC 5 K	5.22E-02	7.97E-02	4.69E+01
IC 5 L	1.21E-01	1.52E-02	1.96E+02
IC 5 M,N...	1.33E-01	2.70E-03	2.29E+02
IC 6 K	8.28E-02	2.50E-03	1.04E+02
IC 7 K	8.43E-02	1.59E-01	1.07E+02
IC 7 L	1.53E-01	2.69E-02	2.90E+02
IC 7 M,N...	1.65E-01	9.40E-03	3.29E+02
Auger KLL	5.50E-02	2.68E-02	5.13E+01
Auger KLX	6.63E-02	1.53E-02	7.08E+01
Auger KXY	7.75E-02	1.50E-03	9.26E+01
CK LLX	7.73E-04	3.22E-01	4.75E-02
Auger LMM	7.58E-03	5.41E-01	1.68E+00
Auger LMX	9.85E-03	2.35E-01	2.63E+00
Auger LX Y	1.20E-02	1.91E-02	3.69E+00
CK MMX	4.06E-04	9.23E-01	1.93E-02
Auger MXY	1.83E-03	2.03E+00	1.67E-01
CK NNX	1.72E-04	4.41E+00	8.24E-03
Auger NXY	6.44E-05	7.93E+00	3.99E-03
CK OOX	4.53E-05	2.84E+00	3.01E-03
Auger OXY	1.61E-05	1.76E+01	6.83E-04
X-ray K $_{\alpha 1}$	7.08E-02	4.69E-01	
X-ray K $_{\alpha 2}$	6.89E-02	2.74E-01	
X-ray K $_{\beta 1}$	8.03E-02	1.03E-01	
X-ray K $_{\beta 2}$	8.25E-02	3.57E-02	
X-ray K $_{\beta 3}$	7.98E-02	5.15E-02	
X-ray K $_{\beta 4}$	8.27E-02	1.40E-03	
X-ray K $_{\beta 5}$	8.08E-02	3.20E-03	
X-ray KM,N,O	8.25E-02	5.90E-03	
X-ray L	1.10E-02	4.15E-01	
X-ray M	2.24E-03	5.62E-02	

Total yield of Auger and CK electrons per decay=36.9

Total yield of IC electrons per decay= 1.1

Total yield of x-rays per decay= 1.4

Total yield of γ -rays per decay =0.13

Total energy released per decay= 138508 eV

Auger and CK energy released per decay= 15273 eV

IC energy released per decay=30220 eV

X-ray energy released per decay =72947 eV

γ -ray energy released per decay=20068 eV

the conventional ^{125}I spectrum published by the MIRD Committee.¹⁴ The absence of the very low-energy N- and O-shell Auger electrons in this spectrum results in a dose about 3.5 times smaller (Table XIII) than the detailed spectrum in this report (Table VIII). This difference is significant in that it points out the importance of low-energy Auger electrons in small volume dosimetry and confirms that conventional spectra are inadequate for this purpose.

TABLE XII. Pb-203 average radiation spectrum.

	Average energy (MeV)	Yield/decay	Range (microns)
γ_1	2.79E-01	7.99E-01	
γ_2	4.01E-01	3.33E-02	
γ_3	6.81E-01	9.00E-03	
IC 1 K	1.94E-01	1.32E-01	4.28E+02
IC 1 L	2.64E-01	3.38E-02	7.03E+02
IC 1 M,N...	2.76E-01	1.14E-02	7.53E+02
IC 2 K	3.16E-01	6.20E-03	9.25E+02
Auger KLL	5.65E-02	2.11E-02	5.38E+01
Auger KLX	6.86E-02	1.07E-02	7.50E+01
Auger KXY	8.01E-02	1.40E-03	9.19E+01
CK LLX	8.97E-04	1.76E-01	5.84E-02
Auger LMM	7.75E-03	4.11E-01	1.75E+00
Auger LMX	1.01E-02	1.80E-01	2.75E+00
Auger LX Y	1.23E-02	1.43E-02	3.86E+00
CK MMX	4.11E-04	6.79E-01	1.96E-02
Auger MXY	1.89E-03	1.53E+00	1.75E-01
CK NNX	1.68E-04	2.36E+00	8.10E-03
Auger NXY	6.95E-05	5.11E+00	4.19E-03
CK OOX	4.69E-05	1.50E+00	3.12E-03
Auger OXY	2.22E-05	1.13E+01	1.13E-03
X-ray K $_{\alpha 1}$	7.29E-02	4.30E-01	
X-ray K $_{\alpha 2}$	7.08E-02	2.57E-01	
X-ray K $_{\beta 1}$	8.26E-02	9.29E-02	
X-ray K $_{\beta 2}$	8.49E-02	3.37E-02	
X-ray K $_{\beta 3}$	8.21E-02	4.77E-02	
X-ray K $_{\beta 5}$	8.31E-02	2.20E-03	
X-ray KM,N,O	8.49E-02	8.40E-03	
X-ray L	1.14E-02	3.42E-01	
X-ray M	2.31E-03	4.51E-02	

Total yield of Auger and CK electrons per decay=23.3
Total yield of IC electrons per decay=0.19
Total yield of x-rays per decay= 1.3
Total yield of γ -rays per decay=0.84
Total energy released per decay=363461 eV
Auger and CK energy released per decay= 11630 eV
IC energy released per decay=40401 eV
X-ray energy released per decay=68897 eV
 γ -ray energy released per decay=242532 eV

B. When are conventional spectra inadequate for dosimetry?

The above findings raise the question as to when detailed spectra, which include the very low-energy Auger electrons, are required for dosimetric purposes. Figure 4 shows the ratio of the doses calculated⁶⁹ using the MIRD spectrum¹⁴ and the present spectrum as a function of the diameter of a spherical volume of unit density matter containing ^{125}I . The ratio ranges from 0.2 for diameters less

TABLE XIII. Dose per unit cumulated activity (Gy/Bq - h) of I-125.

Spectrum	10-nm diameter sphere	20-nm diameter sphere
Sastry and Rao ¹	8.37x 10 ³	1.59x10 ³
Pomplun <i>et al.</i> ⁵	17.4x10 ^{3a}	2.68x10 ^{3a}
MIRD ¹⁴	2.32x10 ³	0.56x10 ³
This report	8.55x10 ³	1.60x 10 ³

^aAssumes all charge potential is deposited within sphere.

TABLE XIV. Se-75 average radiation spectrum (Ref. 32). [Conversion electron, x-ray, and y-ray yields given elsewhere (Ref. 14).]

	Average energy (MeV)	Yield/decay	Range (microns)
Auger KLL } Auger KLX } Auger KXY }	9.48E-03	4.20E-01	2.70E+00
Auger LMM } Auger LMX }	1.18E-03	1.31E+00	8.00E-02
CK LLX } Auger LMM } Auger LMX } CK MMX }	1.47E-04 9.80E-05 4.50E-05 2.90E-05 1.70E-05	1.80E-01 3.70E-01 1.14E+00 2.61E+01 1.35E+00	6.30E-03 4.10E-03 2.00E-03 1.40E-03 1.00E-03

than a few nanometers to 1.0 for diameters greater than about 1 μm . Hence, this suggests that conventional spectra are adequate for calculating absorbed doses to regions having diameters greater than 1 μm . More detailed spectra which include the very low-energy Auger electrons (Tables I-XII, XIV-XVI) are required for smaller volumes. Since the total energy carried by these electrons is small compared to the total energy released by the radionuclide, their importance is limited to microscopic volumes ($< 1 \mu\text{m}$) within which they deposit all of their energy.

C. Complete spectra for other Auger emitters

The small differences (Table XIII) between the absorbed doses calculated with Sastry and Rao's ^{125}I spectrum and the present spectrum (Table VIII) suggest that average spectra calculated using these two methods are roughly equivalent. For the sake of completeness, it is therefore appropriate to include in this report spectra for radionuclides not listed in Tables I-XII which were calculated in the same manner as the ^{125}I spectrum of Sastry and Rao.¹ Accordingly, the Auger electron spectra for ^{51}Cr (Ref. 19), ^{75}Se (Refs. 1 and 32), and ^{77}Br (Refs. 1 and 31) are given in Tables XIV-XVI. It should be noted that x-ray, y-ray, and conversion electron yields and energies

TABLE XV. Br-77 average radiation spectrum (Ref. 31). [Conversion electron, x-ray, and γ -ray yields given elsewhere (Ref. 14).]

	Average energy (MeV)	Yield/decay	Range (microns)
Auger KLL } Auger KLX } Auger KXY }	1.01E-02	3.53E-01	3.10E+00
Auger LMM } Auger LMX }	1.25E-03	1.13E+00	8.00E-02
CK LLX } Auger LMM } Auger LMX } CK MMX }	1.46E-04 8.10E-05 4.20E-05 1.90E-05 2.00E-05	2.80E-02 1.73E+00 1.74E+00 3.40E-01 6.70E-01	7.00E-03 4.70E-03 4.20E-03 1.00E-03 1.00E-03
Continuum	5.00E-06	6.70E-01	

TABLE XVI. Cr-51 average radiation spectrum (Ref. 19). [Conversion electron, x-ray, and γ -ray yields given elsewhere (Ref. 14).]

	Average energy (MeV)	Yield/decay	Range (microns)
Auger KLL } Auger KLX } Auger KXY }	4.38E-03	6.70E-01	6.50E-01
Auger LMM } Auger LMX }	4.49E-04	1.43E+00	2.30E-02
CK LLX } Auger LMM } Auger LMX } CK MMX }	9.10E-05 4.60E-05 2.00E-05 1.10E-05 3.00E-06	1.30E-01 3.10E-01 2.18E+00 5.30E-01 1.70E-01	5.00E-03 3.00E-03 1.00E-03 1.00E-03 5.00E-04

are not listed in Tables XIV-XVI. These data were not provided by the authors and may be obtained from Ref. 14.

V. CONCLUSION

This report provides detailed Auger electron spectra for a number of radionuclides of medical and environmental significance. The complete radiation spectra given in Tables I-XII are largely similar to those of MIRD¹⁴ and ICRP¹⁵ with the exception of the low-energy Auger electron component. The spectra in this report give complete Auger electron spectra including the low-energy M-, N-, and O-shell Auger electrons, thereby offering significantly more detail in this region than do conventional spectra.^{14,15} Dosimetry calculations indicate that the detailed spectra in this report are preferred over conventional MIRD spectra¹⁴ for small volume dosimetry (diameters $< 1 \mu\text{m}$). For larger volumes the spectra are dosimetrically equivalent.

ACKNOWLEDGMENTS

Preparation of this report was supported in part by USPHS Grant No. CA-32877 and New Jersey Cancer Commission Grant No. 688-009. Sven-Erik Strand and Gustav Grafström of the University of Lund, Sweden, provided assistance with the $^{113\text{m}}\text{In}$, $^{115\text{m}}\text{In}$, and ^{203}Pb spectra.

¹James G. Kereiakes, Co-Chairman, Dandamudi V. Rao, Co-Chairman, Roger W. Howell, John L. Humm, Ravinder Nath, Kandula S. R. Sastry, Sven-Erik Strand, and Stephen R. Thomas.

²K. S. R. Sastry and D. V. Rao, "Dosimetry of low energy electrons," in *Physics of Nuclear Medicine: Recent Advances*, edited by D. V. Rao, R. Chandra, and M. Graham (American Institute of Physics, New York, 1984), pp. 169-208.

³D. V. Rao, V. B. Mylavarapu, G. F. Govelitz, V. K. Lanka, K. S. R. Sastry, and R. W. Howell, "Biological and biophysical dosimetry of Auger-emitters in vivo: A Review," in *Selected Topics in Physics of Radiotherapy and Imaging*, edited by U. Madhvanath, K. S. Parthasarathy, T. V. Venkateswaran (Tata McGraw-Hill, New Delhi, 1988), pp. 232-258.

⁴D. V. Rao, V. R. Narra, R. W. Howell, G. F. Govelitz, and K. S. R. Sastry, "In-vivo radiotoxicity of DNA-incorporated I-125 compared with that of densely ionising alpha-particles," *The Lancet* Vol II, No. 8664, 650-656 (1989).

⁵H. A. Wright, R. N. Hamm, J. E. Turner, R. W. Howell, D. V. Rao, and K. S. R. Sastry, "Calculations of physical and chemical reactions with DNA in aqueous solution from Auger cascades," *Radiat. Prot. Dosim.* 31, 59-63 (1990).

- ⁵E. Pomplun, J. Booz, and D. E. Charlton, "A Monte Carlo simulation of Auger cascades," *Radiat. Res.* **111**, 533-552 (1987).
- ⁶D. E. Charlton and J. L. Humm, "A method of calculating initial DNA strand breakage following the decay of incorporated I-125," *Int. J. Radiat. Biol.* **53**, 353 (1988).
- ⁷D. V. Rao, V. R. Narra, R. W. Howell, and K. S. R. Sastry, "Biological consequence of nuclear versus cytoplasmic decays of I-125: Cysteamine as a radioprotector against Auger cascades in vivo," *Radiat. Res.* **124**, 188 (1990).
- ⁸E. Pomplun, "A new DNA target model for track structure calculations and its first application to I-125 Auger electrons," *Int. J. Radiat. Biol.* **59**, 625-642 (1991).
- ⁹R. W. Howell, D. V. Rao, D. Y. Hou, V. R. Narra, and K. S. R. Sastry, "The question of relative biological effectiveness and quality factor for Auger emitters incorporated into proliferating mammalian cells," *Radiat. Res.* **128**, 282-292 (1991).
- ¹⁰R. Loevinger and M. Berman, "A revised schema for calculating the absorbed dose from biologically distributed radionuclides," *MIRD Pamphlet No. 1*, revised (Society of Nuclear Medicine, New York, 1976).
- ¹¹R. Loevinger, T. F. Budinger, and E. E. Watson, *MIRD Primer for Absorbed Dose Calculations* (Society of Nuclear Medicine, New York, 1988).
- ¹²A. I. Kassis, R. W. Howell, K. S. R. Sastry, and S. J. Adelstein, "Positional effects of Auger decays in mammalian cells in culture," in *DNA Damage by Auger Emitters*, edited by K. F. Baverstock and D. E. Charlton (Taylor & Francis, London, 1988), pp. 1-14.
- ¹³R. Nath, P. Bongiomini, and S. Rockwell, "Enhancement of IUDR radiosensitization by low energy photons," *Int. J. Radiation Oncol. Biol. Phys.* **13**, 1071-1079 (1987).
- ¹⁴D. A. Weber, K. F. Eckerman, L. T. Dillman, and J. C. Ryman, *MIRD: Radionuclide Data and Decay Schemes* (Society of Nuclear Medicine, New York, 1989).
- ¹⁵International Commission on Radiation Protection (ICRP), "Radionuclide Transformations," ICRP Publication 38 (Pergamon, Oxford, 1983).
- ¹⁶K. S. R. Sastry, C. Haydock, A. M. Basha, and D. V. Rao, "Electron dosimetry for radioimmunotherapy: Optimal electron energy," *Radiat. Prot. Dosim.* **13**, 249-253 (1985).
- ¹⁷K. S. R. Sastry, R. W. Howell, D. V. Rao, V. B. Mylavarapu, A. I. Kassis, S. J. Adelstein, H. A. Wright, R. N. Hamm, and J. E. Turner, "Dosimetry of Auger-emitters: Physical and phenomenological approaches," in *DNA Damage by Auger Emitters*, edited by K. F. Baverstock and D. E. Charlton (Taylor & Francis, London, 1988), pp. 27-38.
- ¹⁸S. J. Adelstein, A. I. Kassis, and K. S. R. Sastry, "Cellular vs. organ approaches to dose estimates," in *Proceedings of the Fourth International Radiopharmaceutical Dosimetry Symposium*, Oak Ridge, TN, November 1985, DOE Conference, CONF-851113, (DE86010102), edited by A. T. Schlawke-Stelson and E. E. Watson (1986), pp. 13-25.
- ¹⁹A. I. Kassis, K. S. R. Sastry, and S. J. Adelstein, "Intracellular distribution and radiotoxicity of Chromium-51 in mammalian cells: Auger-electron dosimetry," *J. Nucl. Med.* **26**, 59-67 (1985).
- ²⁰A. I. Kassis, K. S. R. Sastry, and S. J. Adelstein, "Kinetics of uptake, retention, and radiotoxicity of ¹²⁵IUDR in mammalian cells: Implications of localized energy deposition by Auger processes," *Radiat. Res.* **109**, 78-89 (1987).
- ²¹R. W. Howell, D. V. Rao, and C. Haydock, "Dosimetry techniques for therapeutic applications of incorporated radionuclides," in *Dosimetry of Incorporated Radionuclides*, edited by S. J. Adelstein, A. I. Kassis, and R. W. Burt (American College of Nuclear Physicians, Washington DC, 1990), pp. 215-256.
- ²²G. M. Makrigrigios, S. J. Adelstein, and A. I. Kassis, "Limitations of conventional internal dosimetry at the cellular level," *J. Nucl. Med.* **30**, 1856-1864 (1989).
- ²³D. E. Charlton, "Calculation of single and double strand DNA breakage from incorporated ¹²⁵I," in *DNA Damage by Auger Emitters*, edited by K. F. Baverstock and D. E. Charlton (Taylor & Francis, London, 1988), pp. 89-100.
- ²⁴D. E. Charlton, H. Nikjoo, and J. L. Humm, "Calculation of initial yields of single- and double-strand breaks in cell nuclei from electrons, protons, and alpha particles," *Int. J. Radiat. Biol.* **56**, 1-19 (1989).
- ²⁵J. L. Humm and D. E. Charlton, "A new calculational method to assess the therapeutic potential of Auger electron emission," *Int. J. Radiation Oncology Biol. Phys.* **17**, 351-360 (1989).
- ²⁶E. Pomplun, J. Booz, A. Dydejczyk, and L. E. Feinendegen, "A microdosimetric interpretation of the radiobiological effectiveness of ¹²⁵I and the problem of quality factor," *Radiat. Environ. Biophys.* **26**, 181-188 (1987).
- ²⁷E. M. Smith, C. C. Harris, and R. H. Rohrer, "Calculation of local energy deposition due to electron capture and internal conversion," *J. Nucl. Med.* **7**, 23-31 (1966).
- ²⁸F. C. Gillespie, J. S. Orr, and W. R. Greig, "Microscopic dose distributions from I-125 in the toxic thyroid gland and its relation to therapy," *Br. J. Radiol.* **43**, 40-47 (1970).
- ²⁹D. E. Charlton, "Fluorescence photon and Auger electron spectra," *Radiat. Res.* **50**, 455-463 (1972).
- ³⁰D. E. Charlton and J. Booz, "A Monte Carlo treatment of the decay of ¹²⁵I," *Radiat. Res.* **87**, 10-23 (1981).
- ³¹A. I. Kassis, S. J. Adelstein, C. Haydock, K. S. R. Sastry, K. D. McElvany, and M. J. Welch, "Lethality of Auger electrons from the decay of bromine-77 in the DNA of mammalian cells," *Radiat. Res.* **90**, 362-373 (1982).
- ³²A. I. Kassis, S. J. Adelstein, C. Haydock, and K. S. R. Sastry, "Radiotoxicity of Se-75 and S-35: Theory and application to a cellular model," *Radiat. Res.* **84**, 407-425 (1980).
- ³³D. V. Rao, G. F. Govelitz, and K. S. R. Sastry, "Radiotoxicity of thallium-201 in mouse testes: Inadequacy of conventional dosimetry," *J. Nucl. Med.* **24**, 145-153 (1983).
- ³⁴A. I. Kassis, S. J. Adelstein, C. Haydock, and K. S. R. Sastry, "Thallium-201: An experimental and a theoretical radiobiological approach to dosimetry," *J. Nucl. Med.* **24**, 1164-1175 (1983).
- ³⁵A. I. Kassis, F. Fayad, B. M. Kinsey, K. S. R. Sastry, and S. J. Adelstein, "Radiotoxicity of an I-125 labeled DNA intercalator in mammalian cells," *Radiat. Res.* **118**, 283-294 (1989).
- ³⁶G. M. Makrigrigios, A. I. Kassis, J. Baranowska-Kortyiewicz, K. D. McElvany, M. J. Welch, K. S. R. Sastry, and S. J. Adelstein, "Radiotoxicity of 5-[I-123]Iodo-2'-deoxyuridine in V79 cells: A comparison with 5-[I-125]Iodo-2'-deoxyuridine," *Radiat. Res.* **118**, 532-544 (1989).
- ³⁷D. V. Rao, K. S. R. Sastry, G. F. Govelitz, H. E. Grimmond, and H. Z. Hill, "In vivo effects of Iron-55 and Iron-59 on mouse testes: Biophysical dosimetry of Auger electrons," *J. Nucl. Med.* **26**, 1456-1465 (1985).
- ³⁸F. D. Moore and K. S. R. Sastry, "Intracellular potassium: K-40 as a primordial gene irradiator," *Proc. Natl. Acad. Sci. USA* **79**, 3556-3559 (1982).
- ³⁹J. L. Humm, "The analysis of Auger electrons released following the decay of radioisotopes and photoelectric interactions and their contribution to energy deposition," Ph.D. thesis, Polytechnic of the South Bank, London, 1983.
- ⁴⁰J. L. Humm and D. E. Charlton, "Double strand breakage in DNA produced by the photoelectric interaction with incorporated 'cold' bromine," in *DNA Damage by Auger Emitters*, edited by K. F. Baverstock and D. E. Charlton (Taylor & Francis, London, 1988), pp. 111-122.
- ⁴¹R. W. Howell, K. S. R. Sastry, H. Z. Hill, and D. V. Rao, "Cis-platinum-193m: Its microdosimetry and potential for chemo-Auger combination therapy of cancer," in *Proceedings of the Fourth International Radiopharmaceutical Dosimetry Symposium*, Oak Ridge, TN, November 1985, DOE Conference, CONF-851113 (DE86010102), edited by A. T. Schlawke-Stelson and E. E. Watson (1986), pp. 493-513.
- ⁴²D. V. Rao, K. S. R. Sastry, H. E. Grimmond, R. W. Howell, G. F. Goveiitz, V. K. Lanka, and V. B. Mylavarapu, "Cytotoxicity of some indium radiopharmaceuticals in mouse testes," *J. Nucl. Med.* **29**, 375-384 (1988).
- ⁴³J. P. Desclaux, "A multiconfiguration relativistic Dirac-Fock program," *Comp. Phys. Comm.* **9**, 31-45 (1975).
- ⁴⁴T. Tamura, Z. Matumoto, and M. Ohshima, "Nuclear Data Sheets for A=125," *Nuclear Data Sheets* **32**, 497 (1981).
- ⁴⁵M. H. Chen, B. Crasemann, and H. Mark, "Relativistic radiationless transition probabilities for atomic K- and L-shells," *Atomic Data and Nuclear Data Tables* **24**, 13-37 (1979).
- ⁴⁶E. J. McGuire, "M-shell Auger, Coster-Kronig, and radiative matrix elements, and Auger and Coster-Kronig transition rates in j-j coupling," *Res. Rep. SC-RR-710835* (Sandia Laboratories, 1972).
- ⁴⁷E. J. McGuire, "N-shell Auger, Coster-Kronig, and radiative matrix elements, and Auger and Coster-Kronig transition rates in j-j coupling," *Res. Rep. SAND-75-0443* (Sandia Laboratories, 1975).
- ⁴⁸D. C. Kocher, "Nuclear Data Sheets for A=55," *Nuclear Data Sheets* **18**, 463 (1976).

- ⁴⁹J.N. Mo and S. Sen, "Nuclear Data Sheets for $A=67$," Nuclear Data Sheets 39, 741 (1983).
- ⁵⁰B. Harmatz, "Nuclear Data Sheets for $A=111$," Nuclear Data Sheets 27,453 (1979).
- ⁵¹T. Tamura, Z. Matumoto, K. Miyano, and S. Ohya, "Nuclear Data Sheets for $A=123$," Nuclear Data Sheets 29, 453 (1980).
- ⁵²M. R. Schmorak, "Nuclear Data Sheets for $A=201$," Nuclear Data Sheets 25, 193 (1978).
- ⁵³M.R. Schmorak, "Nuclear Data Sheets for $A=203$," Nuclear Data Sheets 24, 117 (1978).
- ⁵⁴M.J. Martin and P. H. Blichert-Toft, "Radioactive atoms, Auger-electron, alpha-, beta-, gamma-, and X-ray data," Nuclear Data Tables A 8, 1-198 (1970).
- ⁵⁵F. Rösler, H. M. Fries, K. Alder, and H. C. Pauli, "Internal conversion coefficients for all atomic shells," Atomic Data and Nuclear Data Tables 21, 291-514 (1978).
- ⁵⁶J. H. Scofield, "Relativistic Hartree-Slater values for K and L X-ray emission rates," Atomic Data and Nuclear Data Tables 14, 121-137 (1974).
- ⁵⁷S. T. Manson and D. J. Kennedy, "X-ray emission rates in the Hartree-Slater approximation," Atomic Data and Nuclear Data Tables 14,111-120 (1974).
- ⁵⁸W. Bambynek, B. Crasemann, H. U. Fink, H. Freund, H. Mark, C. D. Swift, R. E. Price, and P. V. Rao, "X-ray fluorescence yields, Auger and Coster-Kronig transition probabilities," Rev. Mod. Phys. 44,716 813 (1972).
- ⁵⁹L.R.Medsker, "Nuclear Data Sheets for $A=99$," Nuclear Data Sheets **12,431 (1974)**.
- ⁶⁰J. Lyttkens, K. Nilson, and L. P. Ekstrom, "Nuclear Data Sheets for $A=113$," Nuclear Data Sheets 33, 1 (1981).
- ⁶¹B. Harmatz, "Nuclear Data Sheets for $A=115$," Nuclear Data Sheets 30, 413 (1980).
- ⁶²V. S. Shirley, "Nuclear Data Sheets for $A=193$," Nuclear Data Sheets 32, 593 (1981).
- ⁶³B. Harmatz, "Nuclear Data Sheets for $A=195$," Nuclear Data Sheets 23, 607 (1978).
- ⁶⁴K. D. Sevier, *Low Energy Electron Spectrometry* (Wiley Interscience, New York, 1972), pp. 356.
- ⁶⁵M.F. Chung and L. H. Jenkins, "Auger electron energies of the outer shell electrons," Surf. Sci. 22, 479-485 (1970).
- ⁶⁶M.O. Krause and T. A. Carlson, "Vacancy cascade in the reorganization of krypton ionised in-an inner shell," Phys. Rev. 158, 18-24 (1967).
- ⁶⁷T. A. Carlson and R. M. White, "Formation of fragment ions from CH-3Te-125 and C-2H-5Te-125 following the nuclear decays of CH-31-125 and C-2H-51-125," J. Chem. Phys. 38, 2930-2934 (1964).
- ⁶⁸A. Cole, "Absorption of 20 eV to 50,000 eV electron beams in air and plastic," Radiat. Res. 38, 7-33 (1969).
- ⁶⁹R. W. Howell, D. V. Rao, and K. S. R. Sastry, "Macroscopic dosimetry for radioimmunotherapy: Nonuniform activity distributions in solid tumors," Med. Phys. 16, 66-74 (1989).